Materials Horizons

ROYAL SOCIETY OF CHEMISTRY

REVIEW

View Article Online
View Journal | View Issue

Cite this: *Mater. Horiz.*, 2024, **11**, 3500

Unraveling nanosprings: morphology control and mechanical characterization

Dahai Yang,†[a] Rui Huang,†[a] Bolin Zou,[a] Ruoxu Wang,[c] Yong Wang,[d] Edison Huixiang Ang *[b] and Xiaohui Song *[a]

Nanosprings demonstrate promising mechanical characteristics, positioning them as pivotal components in a diverse array of potential nanoengineering applications. To unlock the full potential of these nanosprings, ongoing research is concentrated on emulating springs at the nanoscale in terms of both morphology and function. This review underscores recent advancements in the field and provides a comprehensive overview of the diverse methods employed for nanospring preparation. Understanding the general mechanism behind nanospring formation lays the groundwork for the informed design of nanosprings. The synthesis section delineates four prominent methods employed for nanospring fabrication: vapor phase synthesis, templating methods, post-treatment techniques, and molecular engineering. Each method is critically analyzed, highlighting its strengths, limitations, and potential for scalability. Mechanical properties of nanosprings are explored in depth, discussing their response to external stimuli and their potential applications in various fields such as sensing, energy storage, and biomedical engineering. The interplay between nanospring morphology and mechanical behavior is elucidated, providing insights into the design principles for tailored functionality. Additionally, we anticipate that the evolution of state-of-the-art characterization tools, such as *in situ* transmission electron microscopy, 3D electron tomography, and machine learning, will significantly contribute to both the study of nanospring mechanisms and their applications.

Received 28th April 2024,
Accepted 5th June 2024

DOI: 10.1039/d4mh00503a

rsc.li/materials-horizons

[a] *School of Materials Science and Engineering, Hefei University of Technology, Anhui Province, 230009, China. E-mail: xiaohuisong@hfut.edu.cn*
[b] *Natural Sciences and Science Education, National Institute of Education, Nanyang Technological University, Singapore 637616, Singapore. E-mail: edison.ang@nie.edu.sg*
[c] *Department of Chemistry, School of Science, Westlake University, 600 Dunyu Road, Hangzhou, Zhejiang Province 310030, China*
[d] *Institute for Energy Research, Jiangsu University, Zhenjiang, Jiangsu 212013, P. R. China*
† These authors contributed equally.

Edison Huixiang Ang

Edison Huixiang Ang is currently an Assistant Professor at the National Institute of Education/Nanyang Technological University. He is also an Early Editorial Board Member of Chemical Engineering Journal, Young Editorial Board Member of the Journal of Energy Chemistry, Community Board Member of Materials Horizons, and Associate Editor of Scientific Reports and Frontiers in Chemistry. His current research interests combine nanotechnology and materials science approaches to develop functional nanostructures for advanced energy storage, membrane technology, catalysis, and sensing applications.

Xiaohui Song

Xiaohui Song got his PhD from Nanyang Technological University, Singapore, in 2016. Then he did postdoctoral training at UIUC and UC-Berkeley from 2016 to 2020. Currently, Dr Song is an associate professor of Material Science and Engineering at Hefei University of Technology, China. His research focuses on nanosynthesis, in situ liquid phase nanoscopic imaging, and atomic resolution electron tomography technique, which is used to study hybrid nanomaterials physical and chemical properties.

Wider impact

Our review manuscript comprehensively discusses recent advancements in nanospring fabrication and characterization, focusing on synthesis methods, mechanical properties, and future directions. Key developments include critical evaluations of vapor phase synthesis, templating methods, and molecular engineering of crystal surfaces, shedding light on their strengths and limitations. The significance of nanosprings lies in their unique morphologies and mechanical properties, offering immense potential for applications in sensing, energy storage, and biomedical engineering. The review highlights the importance of understanding the relationship between nanospring morphology and mechanical behaviour, providing insights into tailored functionality design for specific applications. Future directions in nanospring research include molecular engineering, surface ligand chemistry, and advancements in nanosynthesis, with *in situ* transmission electron microscopy (TEM) techniques and TEM 3D tomography emerging as promising tools. This review contributes to shaping materials science by providing a roadmap for precise control over nanospring morphology and properties, driving innovations in nanotechnology and addressing current technological challenges.

1. Introduction

A spring is an elastic object designed to store and release mechanical energy. Typically crafted from resilient metal, its mechanical function involves deformation and recovery of shape upon the application and removal of external force. Various types of springs exist, each serving distinct purposes. The helical spring is a classic example, characterized by its unique helical configuration, capable of shortening or lengthening to store axial force. Widely employed in vehicle suspension and force measurement, it remains a staple in practical applications. Another type is the torsion spring, formed by coiling wire into a tight ring and allowing its ends to rotate, thereby storing torque or twisting force. Commonly found in clips, it serves specific mechanical functions. The hairspring, a coplanar spiral wire, finds extensive use in mechanical watches and marine chronometers due to its design. Additionally, compressed gas utilized in pneumatic shock absorbers can be considered a type of gas spring. Consequently, springs are not confined to helical or spiral shapes; they can be broadly defined as any object with the capability to store and release mechanical energy. Even a bow or a bow-shaped object, composed of a simple resilient rod, can be classified as a spring. A shared focus in contemporary nanoscience and nanotechnology revolves around the creation of functional nanodevices. The demand for mechanical components capable of storing and releasing mechanical energy is prevalent in the development of these devices. Consequently, the scientific community is driven to explore nanostructures that can emulate spring functions in nanoscience. Achieving the goal of mechanical energy storage and release at the nanoscale opens up widespread applications in nanoengineering, including incorporation into resonating elements and as innovative reinforcements in high-strain composites.[1,2] Nanosprings, in particular, are anticipated to play a crucial role in the future as functional nano-robots, representing an extreme case of device miniaturization. These nano-robots may derive their movements not only from traditional power sources like engines or batteries but also from the contributions of nanospring components.

Microsprings have seen successful downsized to the microscale. Nevertheless, employing the classical top-down approach for preparing springs at the nanoscale is impractical, presenting a significant challenge. Consequently, researchers are investing more effort into exploring novel techniques for crafting nanosprings.[3] From a morphological standpoint, most springs exhibit distinct structural features such as helicity and periodicity. The creation of nanostructures with specific helical configurations, achieved through structure mimicking, is considered a straightforward approach to realizing springs at the nanoscale. Consequently, the focus lies predominantly on generating helical, spiral, or coiled nanostructures.

In general, helical, spiral, or coiled structures all consist of wires or belts. Initial experimental evidence suggests that such nanostructures can be observed in nanowire/nanobelt synthesis systems. The correlation between springs and 1D wire/belt structures encourages researchers to explore a nano-spring synthetic strategy analogous to the synthesis of 1D nanostructures. Over the past two decades, a substantial number of helical nanosprings have been synthesized from nanowires/nanobelts. These successful fabrication methods serve as model systems to investigate factors influencing nanospring formation. Simultaneously, the obtained nanosprings are expected to contribute to the study of nanospring behaviour and provide valuable insights into potential applications, including micro-electromechanical systems (MEMS), motors, electromagnets, generators, and related equipment. From a functional perspective, any nanoobject with the capability to store and release mechanical energy is regarded as a nanospring. Consequently, the scope of nanosprings has broadened, extending beyond helical or other conventional spring morphologies. They can be designed with various morphologies exhibiting spring properties, including a bent nanorod capable of storing mechanical energy.[4,5] In addition to a diverse array of structural nanosprings, considering functional aspects opens up new avenues for nanospring design, enabling the functionalization of springs at the nanoscale.

This feature article provides an overview of different methods used in fabricating springs at the nanoscale. Emphasizing facile and flexible fabrication routes as crucial to producing uniform nanosprings, the main focus of this paper is on widely employed strategies. While substantial work has been conducted on organic helical nanostructures, such as DNA helices, this paper does not cover the specific case of organic springs. Instead, the primary focus is on inorganic materials, given their general resilience compared to organic materials. It is essential to note that nanosprings are not confined to classic helical

structures; we also explore the potential for functional springs. The goal of this feature article is not to present an exhaustive literature review but to provide a cohesive discussion of main strategies and the most potentially significant developments in the field of nanosprings.

2. Helical nanosprings morphology control

Helical nanosprings have been extensively investigated through different strategies as shown in Fig. 1 including vapor phase synthesis, a method wherein the precursor materials for nanospring formation exist as gas species, template, molecular engineering, and self-assembly method. These unique anisotropic growth mechanisms result in the formation of helical nanosprings.

2.1. Helical nanosprings from the vapor phase

Helical nanosprings have been extensively investigated through vapor phase synthesis, a method wherein the precursor materials for nanospring formation exist as gas species. The unique anisotropic growth mechanisms result in the formation of helical nanosprings. This discussion centers on the mechanisms governing the formation of anisotropic helical structures, influenced by factors such as catalyst selection, growth conditions, and material chemistry. Of all the vapor-based techniques, those utilizing the vapor–liquid–solid (VLS) mechanisms represent the earliest successful attempts to produce a substantial quantity of helical nanosprings. Wanger initially proposed the VLS process in the 1960s for synthesizing microscale whiskers, and it has since been widely employed in the synthesis of nanowires and nanorods from various materials. However, since the helical structure indicates a highly

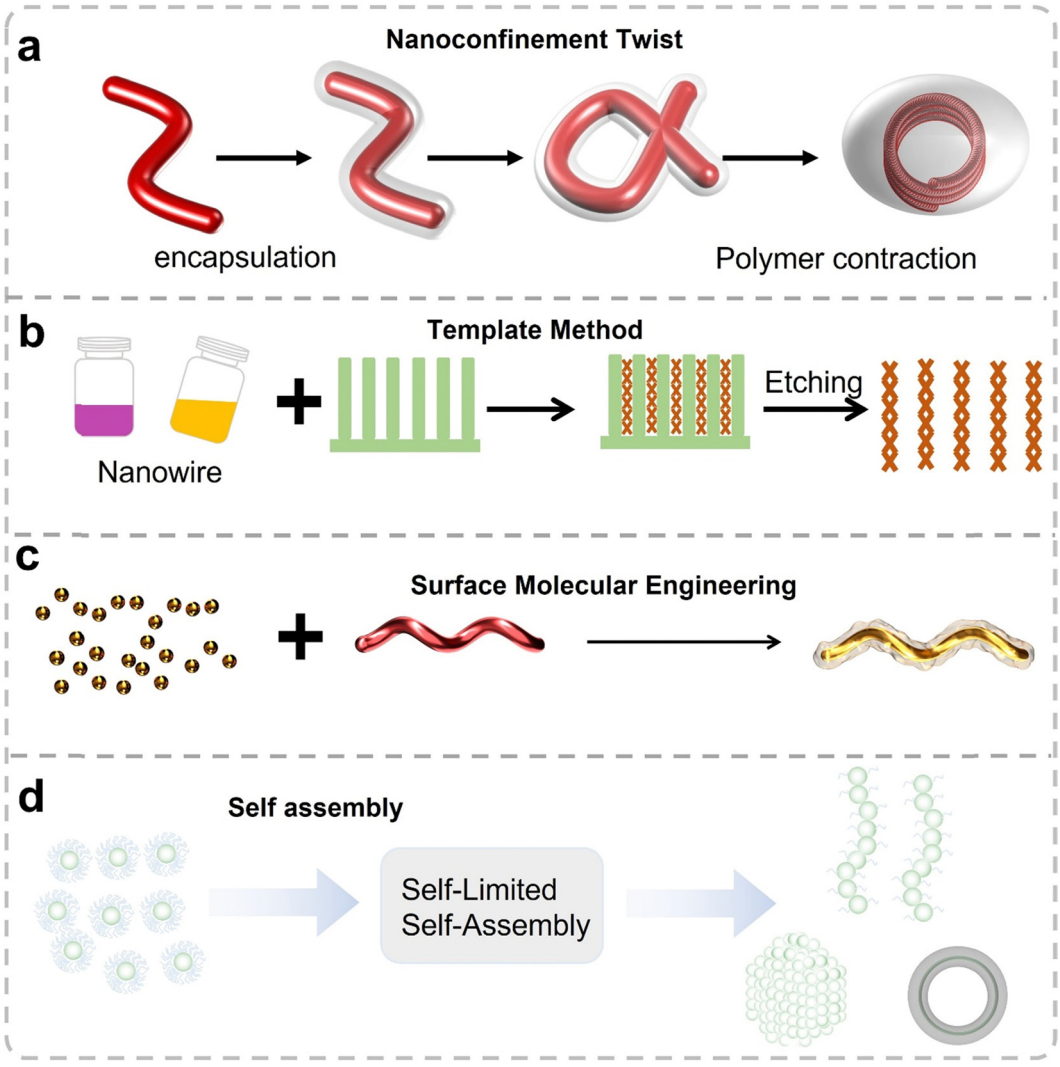

Fig. 1 Schematics of practical spring types, including (a) a schematic diagram showing the result of restricting nanowire growth using a polymer to form specific helical spring shapes. (b) the nanowire structures are grown using the template method to achieve specific morphologies. (c) illustrates the synthesis of nanowires with particular shapes through surface molecular engineering. (d) the formation of nanowire structures with different morphologies regulated by the self-assembly of polymers.

asymmetric growth model, the classical VLS mechanism falls short of providing a comprehensive explanation for the anisotropic growth. Recognizing this limitation, the introduction of anisotropy, a crucial factor for nanospring formation, must be incorporated during the synthesis process.

The prevailing consensus is that helical structures are a consequence of anisotropic and inhomogeneous catalyst activity. This phenomenon is exemplified by helical carbon nanotubes and fiber nanostructures, where the nonuniform growth speed at different parts of a catalyst grain results in helical formation.

In the 1970s, Baker and colleagues observed carbon filaments with spiral morphologies using Sn/Fe alloy as a catalyst, attributing the spiral structures to the stress minimization caused by two identical filaments growing from each catalytic particle in opposite directions at different rates.[6] Further insights were gained by Amelinckx *et al.*, who observed coiled carbon nanotubes with cobalt as a catalyst and acetylene as the carbon source.[7] They proposed the concept of a spatial velocity hodograph, indicating that anisotropic rates of carbon deposition at different parts of the catalyst led to the helical structures. Growth-induced stresses, arising from the mismatch between the extrusion velocity by the catalytic particle required to generate a continuous tubular surface and the rate of carbon deposition, resulted in plastic deformation. Based on theoretical and geometric considerations, it is postulated that the helical structure originates from the concurrent positive and negative curvature caused by periodically incorporating pentagon and heptagon pairs into the hexagonal carbon network, minimizing long-range stresses. This mechanism is widely accepted for explaining the high-yield formation of helical carbon nanocoils.[8–10] For example, Hou *et. al*. have got a large scale synthesis of helically coiled CNTs by use of $Fe(CO)_5$ as a floating catalyst precursor (Fig. 2(a)–(c)).[11,12] The growth process is accompanied by a concomitant insertion/formation of pentagon and heptagon pairs into the hexagonal sheet of the growing nanotube, leading to a helical structure. Significantly, a combination of the systems for producing helical[12] and aligned straight carbon nanotubes, large-scale aligned helical carbon nanotube arrays (Fig. 2(d) and (e)),[13–15] and double helices array.[16]

The anisotropic catalyst activity, determined by facets,[18–23] the size of catalytic particles,[24] the adhesive force between the catalyst and carbon,[16,25–27] and reaction temperature,[28] contributes to the formation of helical structures. In addition to helical carbon nanotubes and nanofibers, this anisotropic

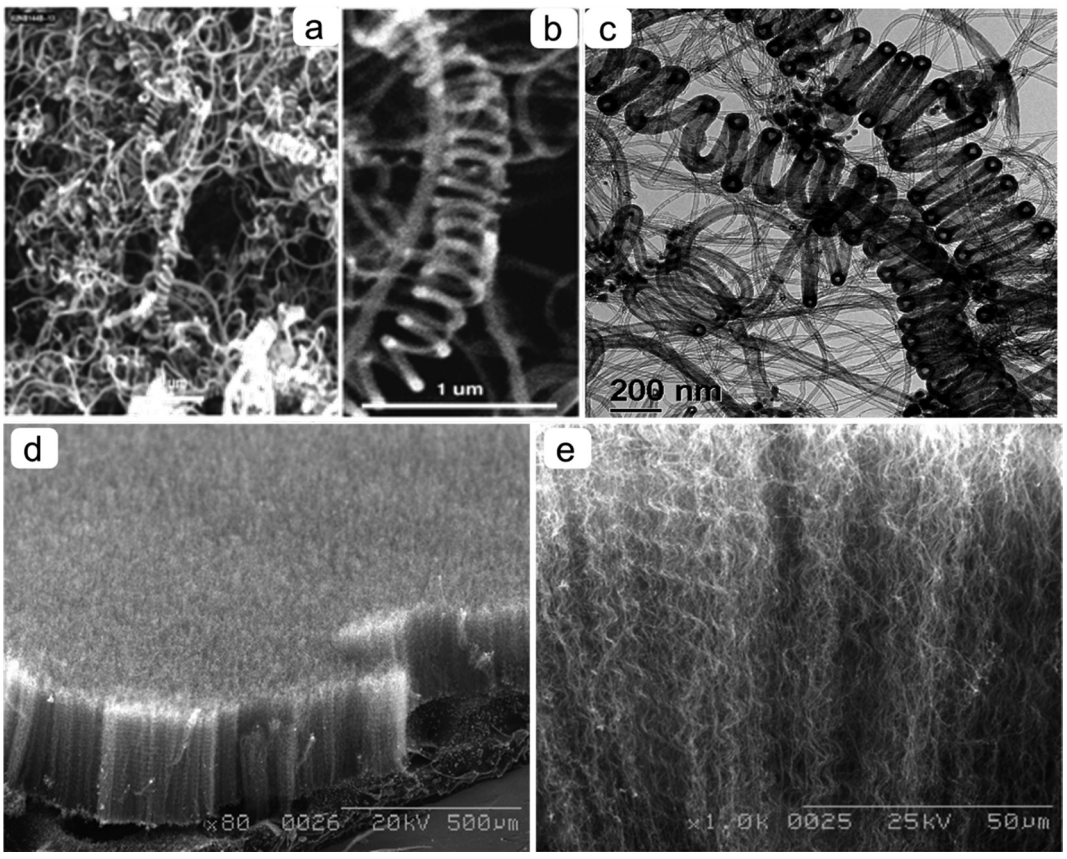

Fig. 2 (a), (b) SEM and (c) TEM images of helical coiled carbon nanotubes prepared by pyrolysis of vapor mixture of $Fe(CO)_5$ and pyridine under H_2 flow at 1050–1150 °C. Reproduced with permission.[17] Copyright 2003, American Chemical Society (d) SEM image of aligned helical carbon nanotube array, and (e) an enlarged cross-section view of (d) showing densely packed aligned helical nanotubes. Reproduced with permission.[11] Copyright 2004 American Chemical Society.

catalyst activity also generates helical nanostructures from various materials. For instance, vapor transport synthesis, assisted by metal nanoparticle catalysts, produced single-crystalline germanium telluride (GeTe) nanohelices.[29] This phenomenon is attributed to differing growth speeds on opposite nanohelical surfaces at the metal–GeTe interface.

Another frequently employed mechanism is contact angle anisotropy (CAA) at the catalyst-nanowire interface, which leads to the asymmetry of the growth front velocity for the obtained nanosprings. Mcllroy *et al.* first proposed this model and successfully prepared amorphous helical boron carbide nanospring (Fig. 3(a)), which resulted from the lateral displacement of the catalyst droplet.[30] Since the CAA model is material independent, it can be general for fabricating helical nanosprings regardless of their composition. Based on this model, SiC,[31] SiO_2,[32] MgB_2,[33] helical nanosprings were also synthesized under the similar conditions (Fig. 3(b)–(d)).[34] In this system, the asymmetry of the growth front stems from the anisotropy in the contact angle at the center of mass of the spherical catalyst droplet concerning the axis of the nascent nanowire. This displacement, in turn, creates an imbalance in surface tension around the catalyst/nanowire interface perimeter. The resulting non-zero torque acting on the catalyst induces a tumbling-like trajectory around the central axis of the resulting nanospring. The essential condition for nanospring growth is that the nanowire's structure, from which the nanospring emerges, must be amorphous.

While several mechanisms have been proposed to explain the formation of helical springs, there is limited conclusive evidence to confirm their plausibility. None of these mechanisms offer predictions or specific reasons for helical growth, maintaining that rather specific conditions would be required for coiling. Dislocations have been also proposed to explain the formation of helical nanospring based on VLS mechanism. Helical crystalline silicon-carried nanowires covered with a silicon oxide shell (SiC/SiO_2) have been synthesized, which the SiC typically had diameters of 10–40 nm with a helical periodicity of 40–80 nm and covered by 30–60 nm amorphous SiO_2.[35] This helical structure originated from an epitaxial growth following the initial screw dislocation sites on the crystalline SiC nanoparticles, and the simultaneous shift and rotation between successive layers were inherent characteristics of crystal screw dislocations and provide the driving force for the helical structure formation. Screw dislocations are common in crystalline materials, and it could be used for the synthesis of silicon[36] and carbon nanohelices Galliumoxide (α-Ga_2O_3)[37] under appropriate experimental conditions. Recently, the Jin group found that screw dislocation-driven nanowire growth also applied to catalyst-free nanowire growth.[38,39] Pine tree-like helical nanowires of lead sulfide (PbS) were synthesized through a vapor phase growth process (Fig. 4). The Cui group also reported a similar helical morphology for lead selenide (PbSe) nanowires.[40] Unlike the vapor–liquid–solid (VLS) mechanism, which requires metal catalysts, this helical nanostructure was formed through a combination of screw dislocation-driven nanowire growth, resulting in long and twisted "trunk" nanowires, and a simultaneous self-catalytic VLS mechanism leading to epitaxial "branch" nanowires.[38–40] Diffraction contrast transmission electron microscopy (TEM) confirmed the presence of dislocations in the trunk, leading to a spiral growth front at the tip of the trunk nanowire, resulting in one-dimensional growth (Fig. 4(h)). Branches grew through a self-catalyst VLS mechanism, with lead nanoparticles generated *in situ* (Fig. 4(i)). The evolution of the highly anisotropic shapes of the helical tree-like structures demonstrated the significant differences in nanowire growth rates between these mechanisms (V_{vls} for VLS, V_s for dislocation-driven, as shown in Fig. 4(k)). The screw component of an axial dislocation provides self-perpetuating steps, enabling one-dimensional crystal growth, a phenomenon known as the Eshelby twist.[41–43]

For a VLS process, the large anisotropic 1D growth of nanostructures is usually generated from the interface between catalyst and nanospring. However, for a VS process without the assistance of a catalyst, the growth of nanostructures is directly dependent on the native structural property of materials. A typical example is Wurtzite ZnO, whose structure can be described as a number of altering planes composed of tetrahedrally coordinated O^{2-} and Zn^{2+} ions, stacked alternately along *c*-axis.

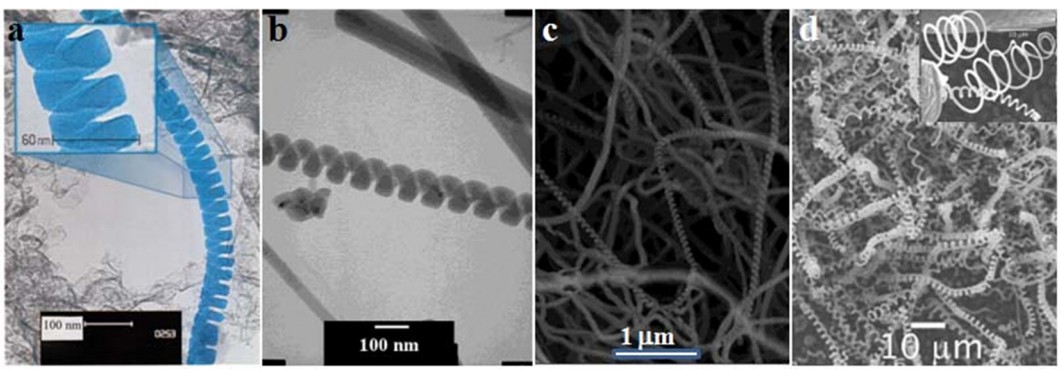

Fig. 3 Bright-field TEM images of (a) an amorphous boron carbide nanospring that has been highlighted for contrast, the inset is a blown-up view of the nanospring, (b) amorphous SiC (silicon carbide) nanosprings, SEM images of (c) as-synthesized SiO_2 (silicon oxide) nanosprings, (d) MgB_2 nanohelices grown on Si substrates, insert shows loosely wound coils. Reproduced with permission.[34] Rights managed by AIP Publishing.

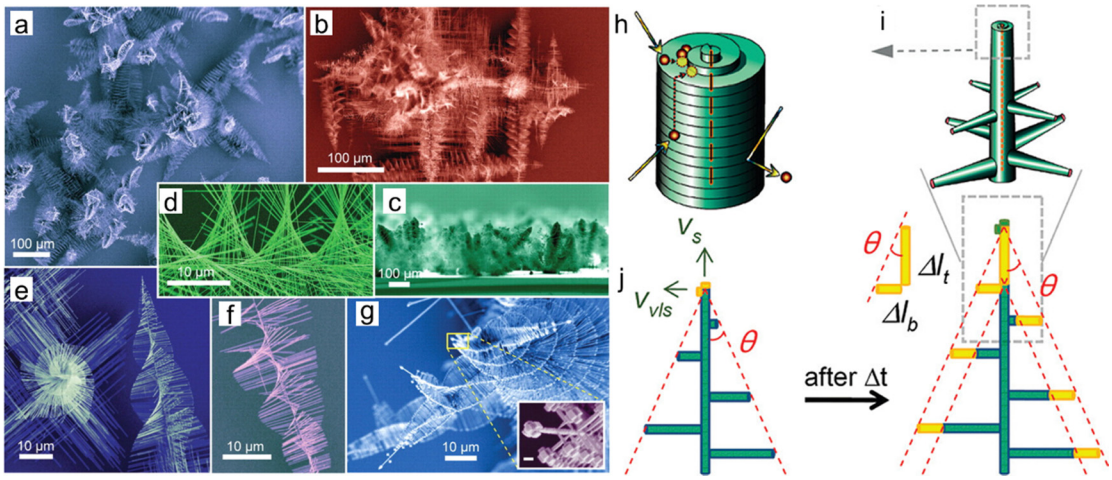

Fig. 4 Left: SEM micrographs of PbS pine tree nanowires. (a) Overview of the dense forest of many nanowire trees. (b) Tree clusters showing epitaxial growth along ⟨100⟩ directions. (c) Side view of growth substrate showing forest growth. (d)–(f) High-magnification views of trees highlight the twisting (Eshelby twist) of the central trunk and helical rotating branches, with (e) further illustrating branch epitaxy on the tree trunk and (f) showing a tree with fewer branches. (g) An example of "tree-on-tree" morphology that can be occasionally observed. Reproduced with permission.[41] Copyright 2008, The American Association for the Advancement of Science. Right: Schematic illustration of the growth process of a PbS helical nanostructure, (h) Anisotropic nanowire growth driven by screw dislocation growth spiral at the magnified trunk tip. (i) Three-dimensional representation of the tip region of a tree highlighting that the fast-growing trunk is driven by a screw dislocation while the branches are driven by VLS mechanism. (j) The tree evolves progressively leading to the formation of a cone angle (θ) of the outer envelope that represents the relative growth rate (trunk *versus* branch, or V_s/V_{vls}) ($\cot\theta$). (Inset) A magnified view of the tips of nanowires after synthesis highlighting the cubes that sometimes decorate the tips. The inset scale bar is 200 nm. Reproduced with permission.[43] Copyright 2009 American Chemical Society.

The positively charged Zn-(0001) and the negatively charged O-(000$\bar{1}$) give a polar surface, leading to a normal dipole moment and spontaneous polarization along the *c*-axis. If the elastic deformation energy is largely suppressed by reducing the thickness of nanobelt or nanowire, the polar nanobelts could change to different shapes such as nanohelices, nanosprials, and nanorings by self-assembly, so that the electrostatic energy coming from the ionic charges on the polar surface can be minimized (Fig. 4).[43]

Wang group presented a series of nanospring, which made of the polar compound ZnO (Fig. 5), showing that the native crystallographic feature plays an important role during the growth of the nanospring structures. By introducing doping, such as In and/or Li, the synthesized ZnO belt, which is dominated by the (0001) polar surface, grows along [2$\bar{1}\bar{1}$0] (the *a*-axis), with its top/bottom surface ±(01$\bar{1}$0) and the side surfaces ±(01$\bar{1}$0). A polar surface can be viewed as a capacitor with two parallel charged plates. Due to the nanobelt's thickness, it easily coils into a sealed ring to minimize electrostatic energy.[44] The stability of nanobelt in the form of a ring or spiral shape is achieved by minimizing the total energy contributed by spontaneous polarization and elasticity.[45,46] As the nanobelt rolls loop-by-loop, helical nanosprings are formed, driven by the repulsive force between charged surfaces and elastic deformation force. These helical nanosprings exhibit a uniform shape with a diameter ranging from 500 to 800 nm, originating from a deformed single-crystal ZnO nanobelt. Additionally, a distinctive helical ZnO nanospring, composed of a superlattice-structured nanobelt, was reported through a vapor–solid (VS) growth process.[47] The as-synthesized helical nanosprings have diameters in the range of 100–500 nm and pitch distances between 500–2500 nm. This helical nanospring consists of a superlattice of striped crystal domains approximately 3.5 nm wide, with alternating crystallographic orientations along the growth direction, specifically [1$\bar{1}$00] and [2$\bar{1}\bar{1}$0]. Each crystal domain stripe has its *c*-axis nearly perpendicular to one another, offset by about 5 degrees, leading to a rigid lattice rotation that causes the ribbon to bend into a helix. In addition to wurtzite structures, anisotropic helical nanosprings induced by polar surfaces were also observed in SnO_2 helical nanosprings with a tetragonal structure,[48] and InP helical nanosprings with a cubic structure.[49]

2.2. Helical nanospring from the templates

As the carbon nanocoils are the most successfully by vapor phase method with good reproducibility and high yields,[50] it has been widely used as a hard template for the fabrication helical nanospring structures. Ueda groups reported that various oxide helical nanotubes, including ZrO_2, Al_2O_3, and SiO_2 could be synthesized by the adsorption and hydrolysis of the oxide precursors on the surface of the carbon nanocoils templates.[51] Similarly, Cui group has successfully deposited continuous and uniform Ni–Fe–Co–P coating on coiled carbon nanofibers *via* electrodeless deposition.[52] However, these simple coating methods cannot achieve convenient and simple control of the thickness and uniformity of the coating because of the low chemical reactivity of templates. A way to this limitation is to use atomic layer deposition, which utilizes the sequential exposure of reactants to substrates to achieve layer-by-layer growth, allowing atomic-scale thickness control.

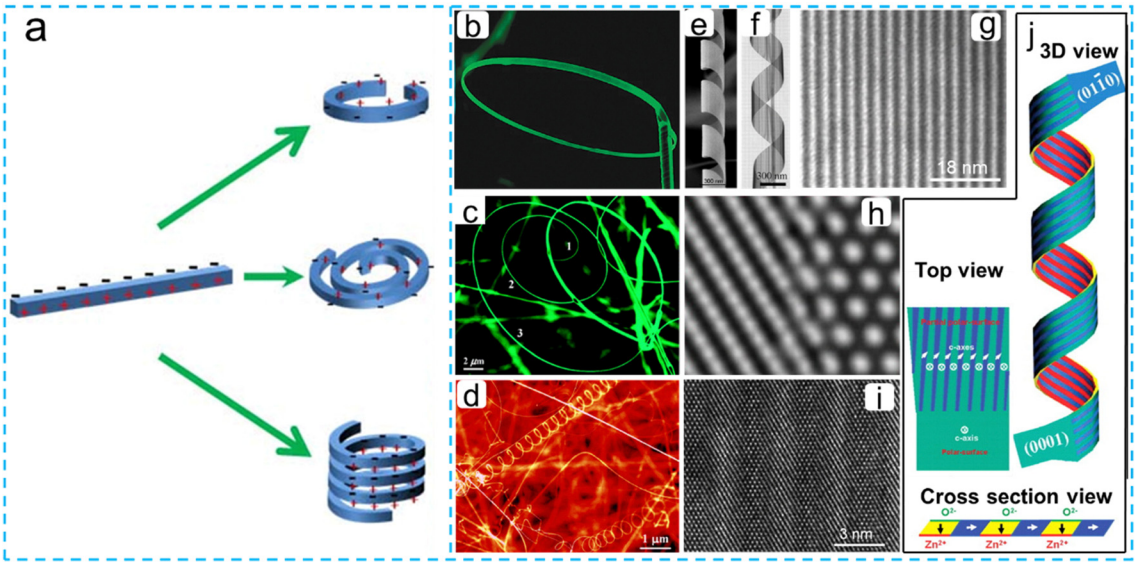

Fig. 5 (a) Proposed growth model showing the initiation and formation of single-crystal ZnO nanostructure with different shapes *via* polar surface induced spontaneous polarization. Right: SEM images of (b) ring, (c) spiral, (d) helical ZnO nanostructure; reproduced with permission.[46] Copyright 2004, American Chemical Society. (e) and (f) SEM and TEM images of ZnO nanohelice. (g)–(i) TEM images at increasing magnification show a superlattice structures of crystalline "stripes" with alternating crystallographic direction. (j) schematic models showing the top view and cross-sectional view of the nanohelice for illustrating the corresponding directions of the c axes and the distribution of polar charges and nonpolar surfaces. Reproduced with permission.[45] Copyright 2005, The American Association for the Advancement of Science.

Various helical oxide nanotubes (Al_2O_3, SiO_2, TiO_2, HfO_2, and $ZnAl_2O_4$) were fabricated by atomic layer deposition using carbon nanocoils as sacrificial templates followed by thermal annealing in air.[53] Moreover, multilayer helical nanotubes were generated through the sequential atomic layer deposition of different materials, providing a means for fabricating nanosprings with hybrid materials.

A comprehensive approach has been developed for creating helical nanostructures with various materials using confined mesoporous silica as a template. In this method, hierarchical mesoporous silica nanostructures within the nanoscale channels of porous anodized alumina are employed as templates. These templates are generated through the integration of electrochemical deposition and a surfactant-induced self-assembly process (Fig. 6(a)–(j)).[54–56] The helical configurations result from the confinement effect, rolling up a parallel array of mesostructured silica cylinders. By adjusting the diameters of the channels in porous anodized alumina, the helical configurations can be controlled, achieving single-helix, double-helix, and core–shell triple-helix structures. The synthesized silica

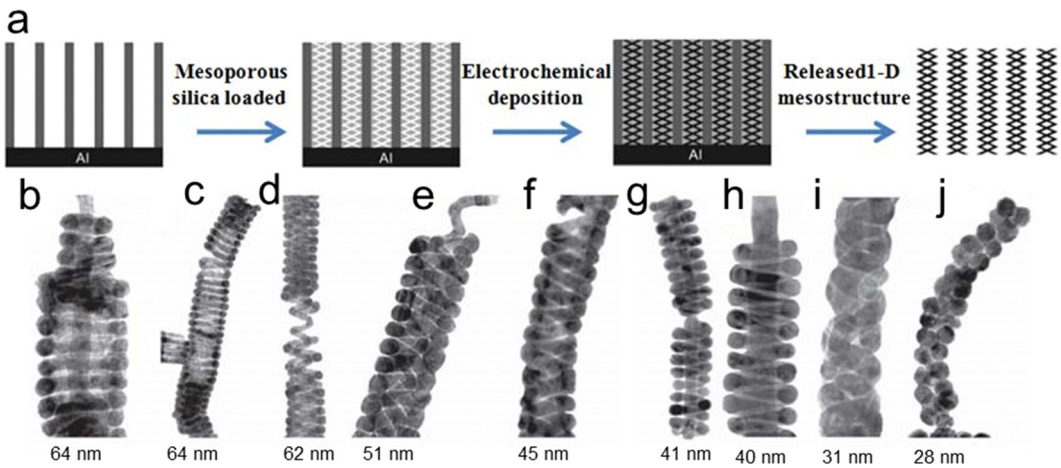

Fig. 6 (a) Preparation procedure of the mesostructured nanosprings using confined mesoporous silica as a template. Bottom: Silver inverted mesostructures prepared by backfilling the confined mesoporous silica, (b) three-layer stacked doughnuts, (c) S-helix, (d) core–shell D-helix, in which the core and the shell are both S-helix, (e) core–shell triple-helix, in which the shell is a D-helix and the core is a S-helix, (f) D-helix, (g), (h) S-helix with a straight core channel, (i) D-helix, (j) inverted peapod structure with two lines of spherical cages packed along the long axis of the alumina nanochannel. Reproduced with permission.[54] Copyright 2004, American Chemical Society.

helix serves as a template for fabricating Ag, Ni, and Cu_2O nanowires with highly ordered hierarchical structures.

In addition to helical carbon nanofibers, helical nanosprings have been successfully prepared through the hybridization of inorganic precursors/block copolymer templates. The Ho group discovered a novel helical phase in the self-assembly of a diblock copolymer containing both achiral and chiral blocks, poly(styrene)-*b*-poly(L-lactide) (PS-PLLA). The formation of this helical phase is attributed to the contribution of the chiral entity (Fig. 7(a)–(c)).[57–59] With the combination of the self-assembly of degradable chiral block copolymer and sol–gel chemistry, three-dimensional ordered helical nanocomposites were obtained. PS with helical nanochannels formed from the self-assembly of the PS-PLLA after hydrolysis, and served as a template. Through the traditional sol–gel reaction that occurred within the template the helical nanocomposites were fabricated.[60]

The soft template method emerges as a highly efficient technique for crafting helical nanosprings. Its superiority lies in its simplicity, particularly in enabling one-pot synthesis, where all components are mixed in a single step. This method boasts versatility in template sources, accommodating various materials to tailor nanospring properties. Notably, it excels in template removal, facilitating a straightforward process through gentle washing at low temperatures. Unlike alternative approaches, the soft template method streamlines fabrication, offering researchers a practical and customizable route to produce nanosprings with desired characteristics. Various groups have reported successful fabrication of helical nanostructures using the soft template method. Shinkai's group, for instance, developed a method for preparing helical structures in silica through the sol–gel polycondensation of tetraethoxysilane (TEOS) onto organic templates within chiral diaminocyclohexane-based organogel systems.[61–63] Their studies showed that the unique helical structures of the organogel fiber can be transcribed in the silica and transition-metal oxide nanostructures. Since then, supramolecular self-assemblies as templates have been widely utilized for the formation of helical nanostructures. Not only the chiral supramolecules,[61–65] but achiral surfactant[66–70] can be used as templates for nanohelices preparation.

For instance, the Huang group reported the formation of well-defined helical nanoribbons through the cooperative effect of multiple weak interactions, such as hydrogen bonds, coordinating interactions, and hydrophobic effects. They successfully

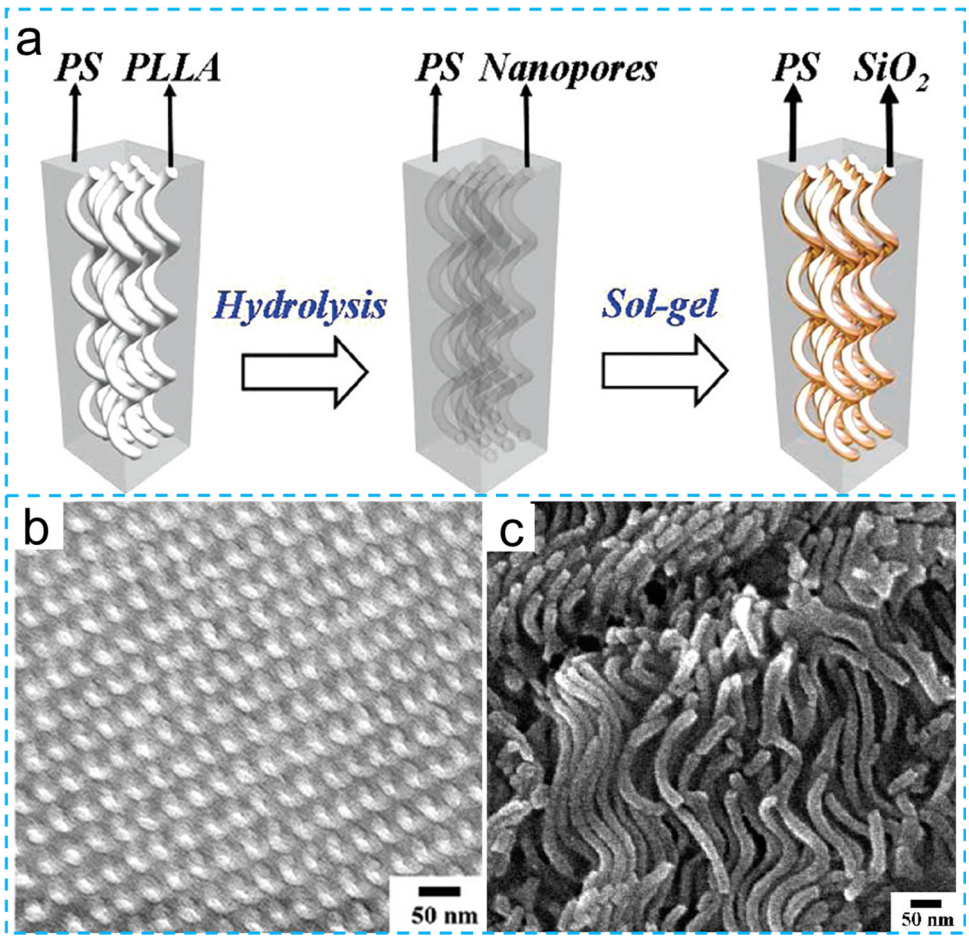

Fig. 7 (a) Schematic illustration of the polymer temptation for generating well-defined helical nanocomposites. Bottom: (b) TEM image of RuO_4 staining PS-PLLA helical nanostructures. (c) SEM image of SiO_2 nanohelices from the PS/SiO_2 helical nanocomposites after the treatment of UV exposure. Reproduced with permission.[57] Copyright 2009, American Chemical Society.

prepared SiO_2 and ZnS helical nanomaterials using a sol–gel process and a self-templating method.[67] Notably, helical silica mesostructures, synthesized in aqueous solutions using soft templates like the triblock copolymer Pluronic F127 and the cationic surfactant cetyltrimethylammonium bromide, were effectively employed as sacrificial templates for generating helical SnO_2 nanotubes.[71] While template methods for helical nanostructures have achieved considerable success, it's important to note that most of these methods are limited to sol–gel reactions. Consequently, the range of materials for synthesized helical nanostructures is restricted, and the amorphous nature of the nanohelices poses a drawback for their potential applications.

2.3. Helical nanospring from post-treatment methods

Exploit an alternative way to roll pre-synthesized nanowire/nanobelt into helical structure can achieve the things that cannot be achieved with a directed growth process. In recent developments, researchers have successfully crafted helical nanospring structures through the controlled self-rolling of strained films. This innovative technique involves a nanometer-thick heteroepitaxial bilayer comprised of SiGe/Si bilayer nanobelts, with the Si layer positioned on top. These bilayers are deposited on a soluble substrate, ensuring that the SiGe layers have consistently smaller thicknesses. Consequently, the stress resulting from lattice misfit is maintained, leading to elastic compression of the SiGe layers. Upon etching away the substrate, the patterned bilayer curls up, releasing internal strain and giving rise to helical spring-like structures (Fig. 8(a)–(c)).[72] This method initiates with stand lithography to pattern films and etches away substrates, offering precise control over the structure, including the turns, thickness, diameter, and pitch of the nanosprings.[73]

To enhance electrical contact, small metal pads are further attached to the ends of these springs, showing potential utility for assembling more intricate nanodevices with self-sensing nanosprings as components.[74] Moreover, this approach demonstrates the capability to extend curling to various nanomaterials; even a polymer film can undergo a similar process by selectively swelling the bottom layer of a polymer or composite-layer film to store mechanical energy.[75–81] In a recent development, silicon nanowire coils were produced through a controlled bulking

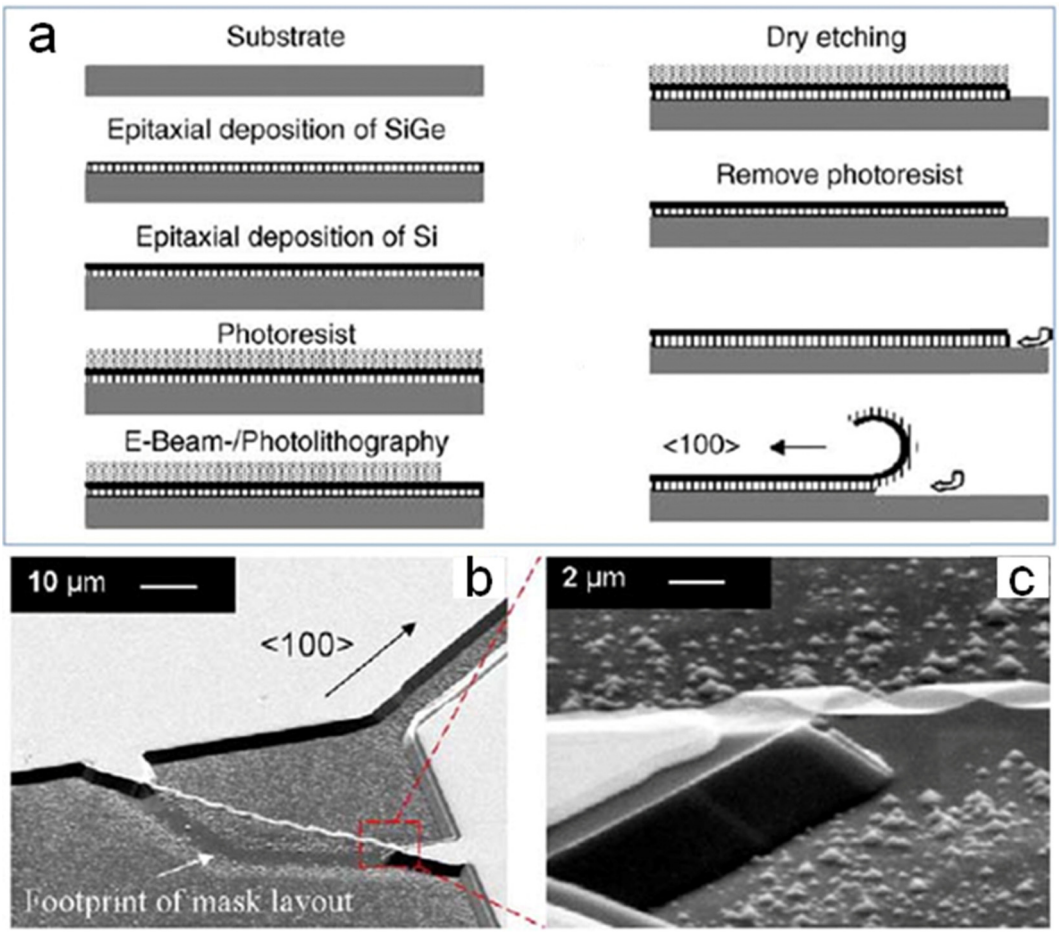

Fig. 8 (a) Schematic of fabrication flow of rolled-up nanospring. Process sequence: an initial planar bilayer patterned through conventional microfabrication techniques assembles itself into 3D nanostructures. This is achieved by controlling the wet etching time so that the loose ends of the nanobelts are located over electrode pads after scrolling. In a subsequent electroplating step, the loose ends are connected to the electrode pads. SEM images of SiGe/Si/Cr helical spring. (b) Fixed on both sides with length of 50 μm, and (c) enlarged view showed the bilayer thickness is 20 nm. Reproduced with permission.[72] Copyright 2005 Elsevier B.V. All rights reserved.

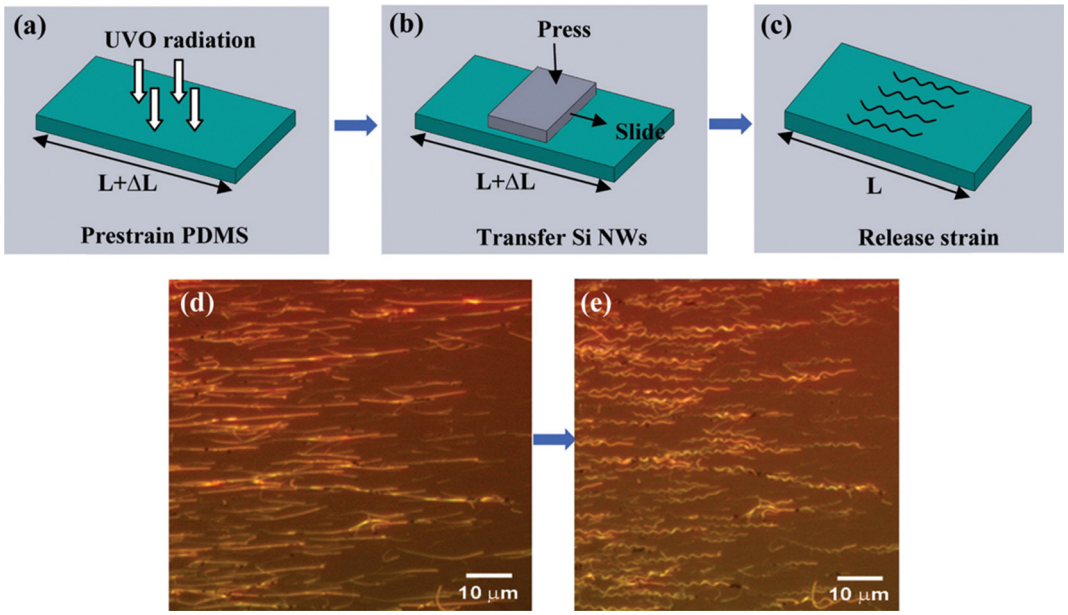

Fig. 9 (a)–(c) Schematic illustration of the process for fabricating the deformed NWs. A large-area optical micrograph of the Si NWs (d) before and (e) after release of the prestrained PDMS substrate. Reproduced with permission.[83] Copyright 2011, American Chemical Society.

process.[82] Fig. 9(a)–(c) shows the Si nanowires were assembled on prestrained poly(dimethylsiloxane) (PDMS) substrates, and releasing the prestrained PDMS through UV radiation led to the buckling of Si nanowires, forming coiled structures. These coiled Si nanowires exhibit significant stretchability, akin to the motion of a coil spring. This approach is also compatible with other materials such as GaAs, GaN, and InP.[83,84]

Capillary force serves as a prevalent driving force for the self-assembly of objects ranging from nanoscale to mesoscale, including helical nanostructures. The fundamental concept of this approach is illustrated in Fig. 10(a) and (b). When an array of straight nanopillars is submerged in liquid and subsequently evaporated, capillary force is generated at the nanopillar-liquid–air interface, leading to the collapse of nanopillars and the formation of nanocohesion.[85] The emergence of helical structures is attributed to the interplay between intrapillar elasticity and interpillar adhesion.[5,86] Based on this capillary force-induce cohesion, Aizenberg group reported self-organization of nanobristle into helical clusters, and they successfully prepared nanotrivial, hierarchically assembled, coiled mesostructures over large areas, and the obtained helical structures may have the ability to store elastic energy and information embodied in adhesive patterns (Fig. 10).[85,87,88] This approach enables the formation of complex helical pattern even at 10 nm length scale,[89] and it believes that this technique can be applied to other high-aspect-ratio nanostructures, such as functional vertically aligned semiconductor nanowires/nanorods, carbon nanotubes or metal nanopillars to perhaps permit functional self-assembled structures.[90]

2.4. Helical nanospring from the metal crystal surface molecular engineering in colloids

The development of helical nanosprings through molecular engineering on metal crystal surfaces in colloids represents a significant advancement in nanomaterial synthesis. By meticulously controlling the molecular structure and interactions at the surface, researchers can engineer the growth process precisely, yielding well-defined helical structures with tailored properties. Our previous work, as depicted in Fig. 11(a)–(e), illustrates the schematics of the coalescence process of Au–Pd nanoropes, synthesized through a modified version of a previously reported method.[91] Initially, ultrathin Au nanowires stabilized by oleylamine were synthesized and phase-transferred into an aqueous solution. Through the deposition of Pd onto these Au nanowire bundles, nanoropes with helical morphologies were obtained. The diffusion of Pd within Au nanowires and the formation of Au–Pd alloy induced lattice transformation, resulting in the twist of the nanowires and coaxial twist of the bundles. In comparison to nanoropes, solid nanowires exhibited reduced diameters. The mechanism involves asymmetric growth within ligand complexes, leading to various helical shapes. Growth initiates from the surface of Au nanoparticles and progresses with time. The untwisting motion of twisted rubber bands serves as a model to comprehend the principles of twisting. Control experiments affirm the necessity of the Au–silica interface and thiolated ligand for nanowire growth. Overall, this study elucidates the growth mechanism of spiral Au nanowires and provides insights into their formation and morphology evolution. This study delves into the intricate mechanisms behind the formation of helical structures from nanowires, with a particular emphasis on two primary twisting modes: self-intertwining and the nanorope mode.

In the self-intertwining mode, individual nanowires intertwine to form double helices with U-turns (Fig. 11(f)), while the nanorope mode results from bundled strands synergistically twisting into straight configurations (Fig. 11(h)).[92] The mechanism

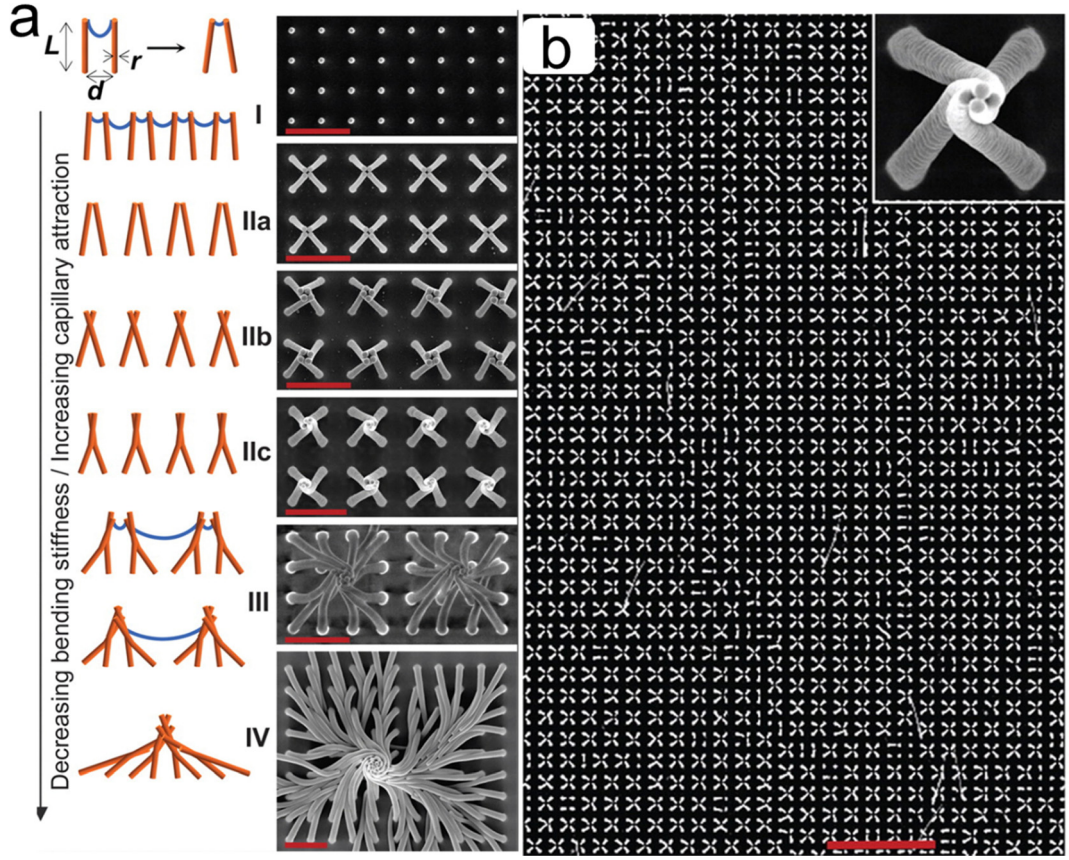

Fig. 10 (a) Schematic diagrams and corresponding SEM images showing the morphogenesis of helical patterns induced by capillary force, from the first-order unclustered nanobristle to the fourth-order coiled bundle. Scale bars, 4 mm. (b) SEM image showing the assembly into uniform, a periodic fourfold cluster of nanopillars over the large area. Reproduced with permission.[85] Copyright 2009, The American Association for the Advancement of Science.

of helix formation bears resemblance to the active surface growth process, but in the unique environment of floccules, asymmetric growth occurs due to the nonuniform deposition of growth materials. Unlike atomically flat substrates that ensure uniform material feeding, floccules exhibit asymmetric blockage and varying extrusion speeds, leading to diverse helicity. Growth plays a crucial role in shaping these helices, with the ligand/diffusion environment influencing anisotropic and asymmetrical growth. It is noteworthy that floccules do not serve as molds for helices; instead, the growth patterns dictate their formation.

An additional illustration of competitive ligands guiding morphology is presented in Fig. 11(j)–(l). Drawing from previous control experiments, helix formation resembles the active surface growth mechanism, albeit with asymmetric growth induced by the unique environment of floccules. Unlike atomically flat substrates ensuring uniform material feeding, floccules exhibit nonuniform growth material deposition due to the asymmetric blockage of seeds. This variation results in diverse helicity as each seed encounters a different environment within the floccules. As nanowires grow, their growth sites within the floccules remain consistent, leading to repeating pitches. The ligand/diffusion environment drives anisotropic and asymmetrical growth, with growth dictating shape.[94,96–98] Contrary to molding, the weaker mechanical strength of floccules suggests they do not universally shape helices. Rare examples illustrate competitive growth, where short helices emerge from nests formed by nanowires. These instances provide insight into helix formation, suggesting that the intertwining of multiple seeds within a pocket can give rise to double or triple helices.

The combination of surface ligand engineering and templates has been developed to design novel nanospring structures.[99,100] The growth process of spiral Au nanowires is depicted in Fig. 11(m). Initially, 40 nm citrate-stabilized Au nanoparticles served as the substrate, onto which aminated 20 nm silica nanoparticles were attached to form the Au–oxide interface. After treating the silica nanoparticles with 3-aminopropyltriethoxylsilane (APTES) to graft the surface with amine groups, concentrated Au nanoparticles were added to the aminated silica solution under vigorous stirring. Nanowire growth was initiated by adding a solution containing the thiolated ligand, 4-mercaptophenylacetic acid (4-MPAA). The obtained Au hybrids exhibited an octopus-like shape (Fig. 11(n) and (o)), with spirals measuring about 60–90 nm in length and diameters gradually decreasing from approximately 19 nm at the root to about 6–7 nm at the tapered end. Trapped intermediates revealed that growth commenced from the surface of Au nanoparticles, with spirals lengthening over

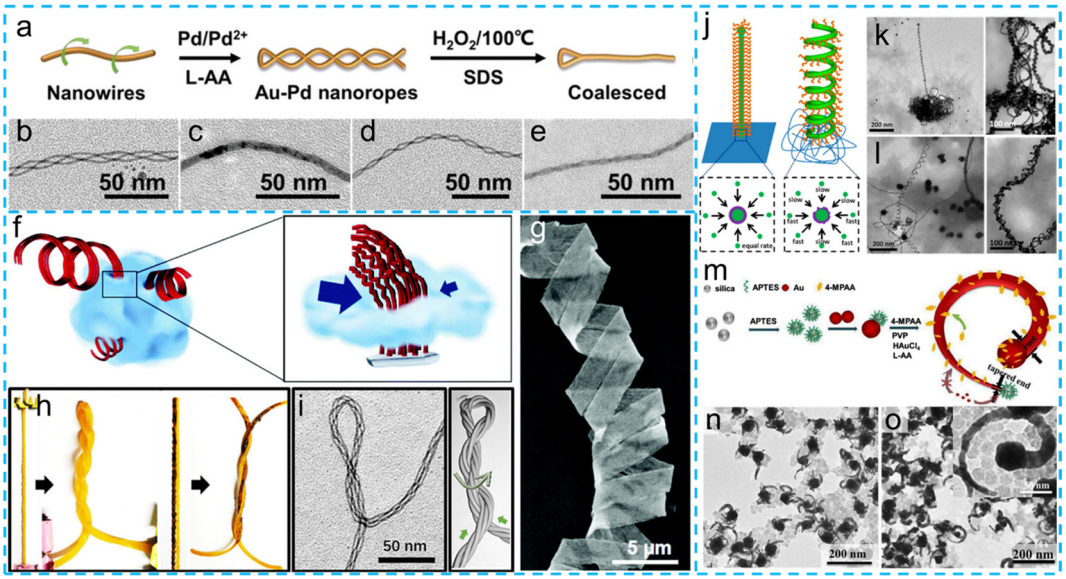

Fig. 11 (a) Schematics illustrating the coalescence of Au–Pd nanoropes. TEM images of typical (b) triple-helical nanoropes, (c) solid nanowires formed by coalescing triple-helical nanoropes, (d) double-helical nanoropes, and (e) solid nanowires formed by coalescing double-helical nanoropes. Reproduced with permission.[91] 2022 Wiley-VCH GmbH. (f) Schematic illustration of the extrusion points and the strain-induced curling mechanism of the helix formation for the nanowire bundles. SEM images showing the nanowire bundles with (g) parallel helices. Rubber band models illustrating. Reproduced with permission.[92] Royal Society of Chemistry 2019. (h) the self-intertwining mode, the nanorope mode, (i) TEM image of a nanorope with the self-intertwined U-turn as the second structure and the corresponding wire model. Reproduced with permission.[93] Copyright 2020 American Chemical Society. Schematics illustrating the different growth modes for (j) straight nanowire on a flat Si wafer and helical nanowire in floccules. The ligands are shown as brown curves. The active site is uniformly accessible in (j) (with an equal rate of atomic deposition shown by the purple circumference) but asymmetrically blocked (with differing rates). (k) Example where a short helix extends out from a ''nest'' made of nanowires. (l) Control experiment where 30 nm Au nanoparticles were introduced as seeds in the growth solution, but no helix was grown on them. Reproduced with permission.[94] Copyright 2017, American Chemical Society. (m) Schematics illustrating the growth mechanism and function of each component in the formation of the spiral Au nanowires, and TEM images of spiral gold nanowires formed with 40 nm Au nanoparticle seeds and 20 nm silica at different growth times: (n) 1 min, (o) 3 min. Reproduced with permission.[95] 2018 Elsevier Inc. All rights reserved.

time, suggesting that controlled growth duration affects nanowire length.[95]

2.5. Coiled nannosprings

In general, nanowires and nanobelts tend to spontaneously assemble into helical, ring, or racket shapes due to the competition between elastic and interfacial effects. Consequently, akin to helical structures, rings formed from coiled nanowires and nanobelts also have the potential to function as nanosprings. Vapor phase synthesis has been applied to the production of ring nanostructures, with carbon nanotube (CNT) nanorings being the most extensively studied (Fig. 12(a) and (b)). During the early stages, CNT rings are typically obtained inadvertently in the process of synthesizing CNTs. The Smalley group first observed CNT rings while characterizing laser-grown single-wall CNTs.[101] The rings exhibit diameters within the range of 300–500 nm and have a height of 1.0–1.2 nm, resembling almost a single continuous toroidal nanotube. The suggested formation mechanism involves a single tube bending around to touch near its ends, and then the two ends adhere to a metal catalyst and become welded together to maximize van der Waals interactions and alleviate bending strain. In contrast to single-tube rings, those composed of well-organized bundles are more prevalent.[102–105] Colomer group found that the double-walled CNT forming rings were not tori but coils, and packed in a triangular arrangement with the bundles.[103] By floating chemical vapor deposition, bundles of SWNT rings have been synthesized, and the yield is higher than 70%.[104] A similar mechanism with helical CNTs may lead to the ring growth.[7] The SWCNT bundles curl up due to the growth-induced stress between the outer and inner nanotubes inside the bundles. This causes the different nanotube chirality to twist against one another.[106–108] As a result, the bundle may be apt to bend to form a curved shape in order to release the stress-energy resulting from the interactions between the nanotubes. Essentially, a balance between tube-tube van der Waals adhesion and the strain energy resulting from coiling-induced curvature is thought to produce the stable nanotube ring structures (Fig. 12(c)–(h)).[109–113]

It should be noted that the formation mechanisms of helical nanostructures from the vapour phase are also applied to coiled nanorings. As illustrated in Section 2, ZnO nanorings were formed based on the polar charge induced self-coiling,[44,46] and SnO_2,[48] GaN[114,115] AlN,[116] ZnSe,[117] $K_2Ti_6O_{13}$,[118] $Na_2Ti_6O_{13}$[119] nanorings also formed by the spontaneous self-coiling of polar nanobelts. Significantly, this mechanism is not applied to vapor phase, but also to the solution phase to generate $Ag_2V_4O_{11}$,[120] $Ag_{1.2}V_3O_8$,[121] and CuO,[122] nanorings under hydrothermal conditions. Bundled Si_3N_4 nanorings were synthesized and structure characterization revealed that the coiled nanowires were bilayer

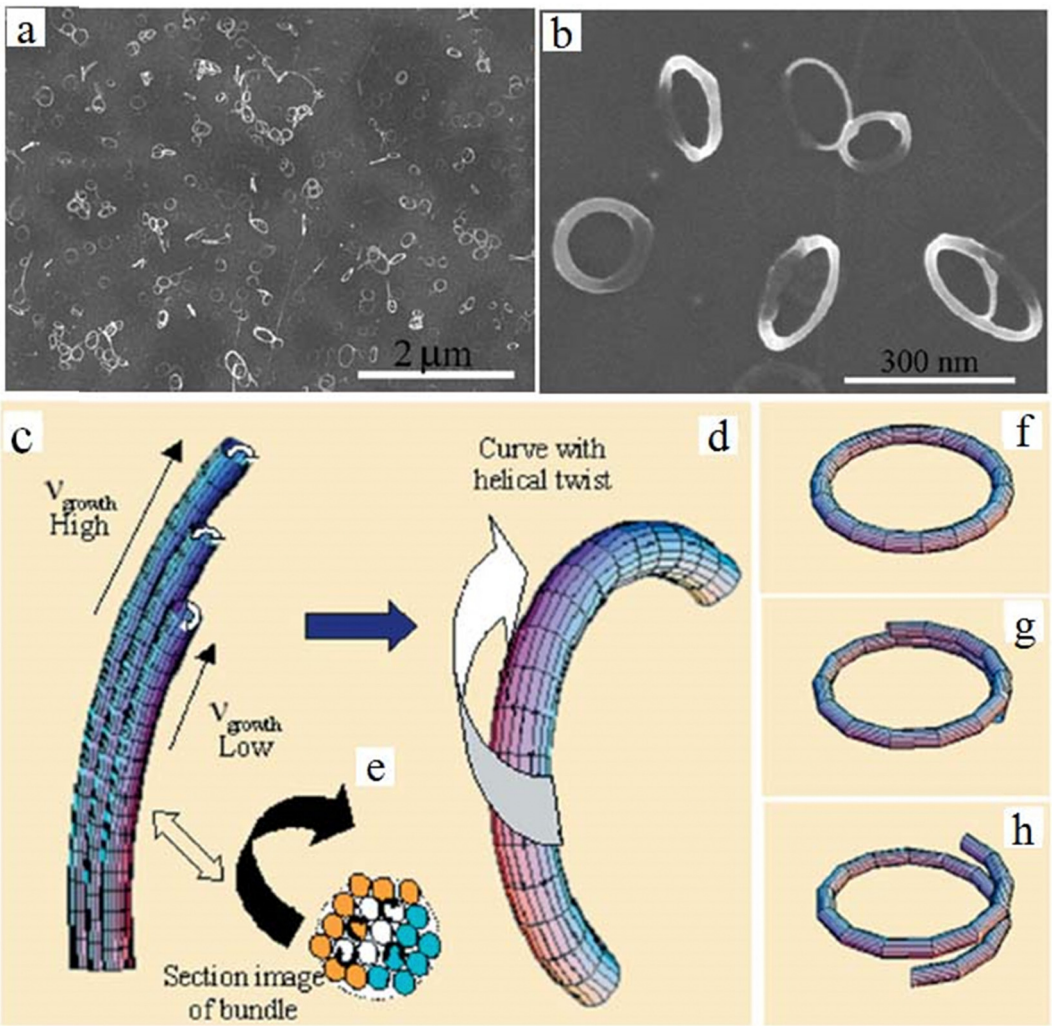

Fig. 12 SEM images of (a) low and (b) high-magnification of SWNT rings. (c)–(h) schematic shows the proposed mechanism for the ring formation. (c), (d) The bundles are induced to twist and bend by the varying growth stress for different nanotubes and due to the tube–tube interactions. (e) Schematic depiction of a cross-section of SWNT bundles showing the varying growth rates of the nanotubes and SWNTs twist against one another. (f)–(h) Possible shapes of bundles resulting from the curling process. Reproduced with permission.[109] Copyright 2006 WILEY-VCH Verlag GmbH & Co. KGaA, Weinheim.

consisting of a crystalline layer and an amorphous layer, therefore the growth rates difference between the two layers caused the nanowire coiled and nanosprings formed.[123]

Post-treatment methods also have been regarded as one of the most power tools to get nanorings. Through an acid treatment coupled with ultrasonic irradiation, single-walled carbon nanotubes (SWCNTs) were induced to self-coil into rings, a process influenced by a delicate balance between tube-tube van der Waals interactions and the strain energy resulting from coiling-induced curvature[111,112,124] Employing a similar methodology, closed SWCNT rings of varying shapes, including circular, oval, and closed ribbon-like structures, were successfully obtained on SiO_2/Si substrates (Fig. 13(a)–(f)).[125,126] The formation of these rings occurred during sonication, and the diverse shapes observed on the substrate can be attributed to the interplay among solvent surface tensions, van der Waals interactions between the rings and the substrate, and the inherent strain forces of the rings. This variety in shapes may also signify the elasticity inherent in CNT rings. Another effective approach for nanoring production involves the chemical functionalization of straight CNTs. By introducing oxygen-containing groups to the ends of cut SWNTs through H_2SO_4/H_2O_2 etching, covalent ring-closure reactions resulted in rings with an average diameter of approximately 540 nm.[127] The Mirkin group successfully achieved the self-assembly of SWNT rings arrays on a gold substrate by integrating dip-pen nanolithography and nano-affinity templates. The strong van der Waals interaction between SWNTs and carboxylic acid moieties attracted the nanotubes to the boundary between a hydrophilic (MUA) and hydrophobic (ODT) self-assembled monolayer on the gold substrate. As a result, long SWNTs coiled into rings at the interface to minimize tension from nanotube bending.[128]

In recent experiments, our group has reported exciting results demonstrating the ability of nanoring structures to

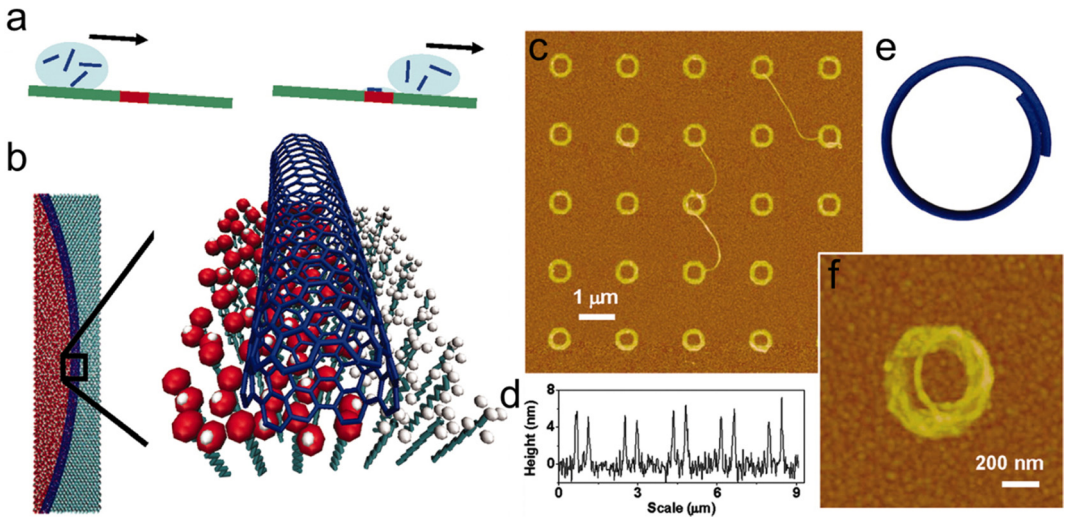

Fig. 13 (a) schematic showing the rolling of a drop of the SWNTs/1,2 dichlorobezene solution on a two-component surface, COOH-SAM (red) and CH_3-SAM (green). (b) The SWNT (blue) are selectively transported to the COOH-SAM and pinned at its boundary with the ODT SAM. Upon drying, the SWNT bends to precisely follow the molecular path of the pattern COOH-SAM. (c) AFM image of SWNT rings and (d) height profiles of SWNT rings, (e), (f) a molecular model and zoom in view of a coiled SWNT ring. Reproduced with permission.[125] Copyright 2006 by The National Academy of Sciences of the USA.

function as nanosprings at the nanoscale. We successfully squeezed ultrathin gold nanowires inside a polymer case, causing them to coil up into tiny springs (Fig. 14(a)).[129] Ultrathin gold nanowires were first encapsulated with a styrene-acrylic acid block copolymer (PSPAA) dissolved in DMF–THF–H_2O, and then a diluted system with water to shrink the polymer shells. The micelle shrinkage triggered the coiling up of the nanowire, and gave a structure resembling that of torsion springs. The two important factors in the process are encapsulation and polymer shell shrinking (Fig. 14(b)–(f)).[130] Since the encapsulating method has successfully extended to various nano-object, it is conceivable that this approach is the potential for generating ring-like nanospring made of various nanowire/nanobelt. Using the modified method, single-wall CNTs were encapsulated in shells of PSPAA and made the CNTs to coil into ring structure by contracting their polymer shells (Fig. 15(a)–(g)).[131] Ultrathin nanowires (NWs) are considered ideal building blocks for assembling intricate nanostructures for future nanodevices. We have illustrated how the polymer/particle duality of ultrathin NWs influences the morphologies of assembled complex nanostructures (Fig. 16(a)). The length of ultrathin AuNWs directly impacts their flexibility, influencing the polymer-like assembly of NWs. Simultaneously, the concentration of surfactants dictates interfacial tension and ligand–solvent interactions, affecting both polymer-like and colloidal assembly of NWs. By precisely adjusting these two factors, ultrathin AuNWs can switch between "soft" and "hard" building blocks, resulting in the formation of highly uniform nanorings, nanograins, nanobundles, and superlattice-like nanospheres (Fig. 16(b)). The distinct assembly behavior of long and short NWs can be viewed as two components for constructing anisotropic complex nanostructures, analogous to the fabrication of polymer–inorganic nanoparticle hybrid nanostructures. We have synthesized anisotropic structures such as Au nanodiamond rings and nanonecklaces by co-assembling polymer-like long NWs with particle-like short NWs or Au nanoparticles.[132]

A new type of coil, the honeycomb, has gained increasing attention due to its promising properties. We report a unique template-free approach for preparing an Au honeycomb monolayer (HMP) film with high transparency and conductivity, as shown in Fig. 16(c). Ultrathin Au nanowires, akin to linear polymer analogues, are directly assembled into the HMP film on various substrates using a traditional static breath figure method. Subsequent chemical cross-linking and oxygen plasma treatment significantly enhance the stability and conductivity of the HMP film (Fig. 16(d)–(g)). The resulting HMP film shows great potential as an ideal candidate for transparent flexible conductive nanodevices.

Beyond the methods mentioned earlier, a 2D coiled-nanospring film, assembled from ultrathin AuAg nanowires, has been successfully created using a straightforward ice-templated assembly technique (Fig. 16(h)). The ice/liquid interface is suggested as a distinctive platform that facilitates the self-assembly of nanowires into monolayer nanofilms. Due to the polymer-like characteristics of ultrathin AuAg nanowires, the resulting ultrathin AuAg nanofilms exhibit remarkable flexibility and stability. These nanofilms, situated on a flexible polyethylene terephthalate substrate, maintain high transparency and conductivity even in challenging environments and under significant deformations. This method, proven successful, can be further extended to produce various complex nanostructures composed of different inorganic ultrathin nanowires.

2.6. Mechanical properties of nanosprings

Measuring the mechanical properties of nanosprings directly is challenging due to their extremely small size, making it difficult

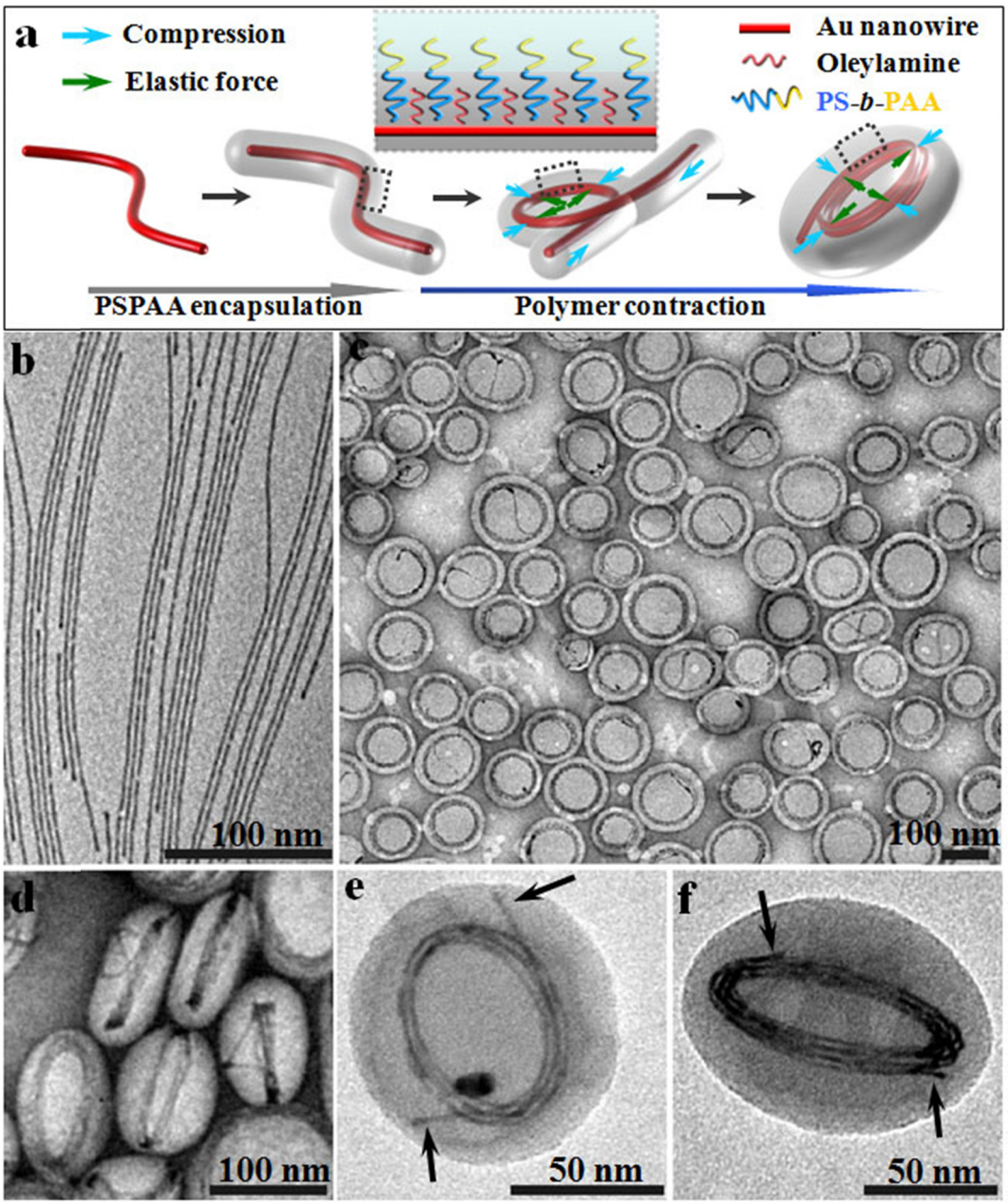

Fig. 14 (a) Schematic showing the polymer-induced coiling of Au nanowires. TEM images of (b) and (d) as-synthesized Au nanowires and coiled nanospring embedded in PSPAA micelles. (d)–(f) typical nanosprings from different perspectives. Reproduced with permission.[130] Copyright 2010, American Chemical Society.

to employ methods used for larger-scale microscopic springs. Therefore, mechanical micromanipulation techniques, integrated with scanning electron microscopy, transmission electron microscopy, and/or atomic force microscopy, are commonly employed to demonstrate the mechanical properties of nanosprings. These instruments enable nanoscale positioning, control, and measurement, addressing the challenges posed by the minute dimensions of nanospring structures.

The elastic properties of coiled carbon nanotubes deposited on oxidized silicon substrates were characterized by AFM and force modulation microscopy (FMM) in the tapping mode, where AFM allowed visualize the helical structure, FMM allowed to probe elasticity along the length of coil.[135] Their results, a Young modulus around 0.7 TPa for the coiled carbon nanotubes, is consistent with the classical theory of elasticity, and comparable to the very high Young modulus of hexagonal graphene sheets. Further study showed this coiled carbon nanotubes can serve as self-sensing mechanical resonators.[136] The device, which is composed of electrical gold contacts attached to the top of helical carbon nanotubes, is connected to a compact radio frequency circuit and allowed to feed an alternating current into the helical carbon nanotubes and to

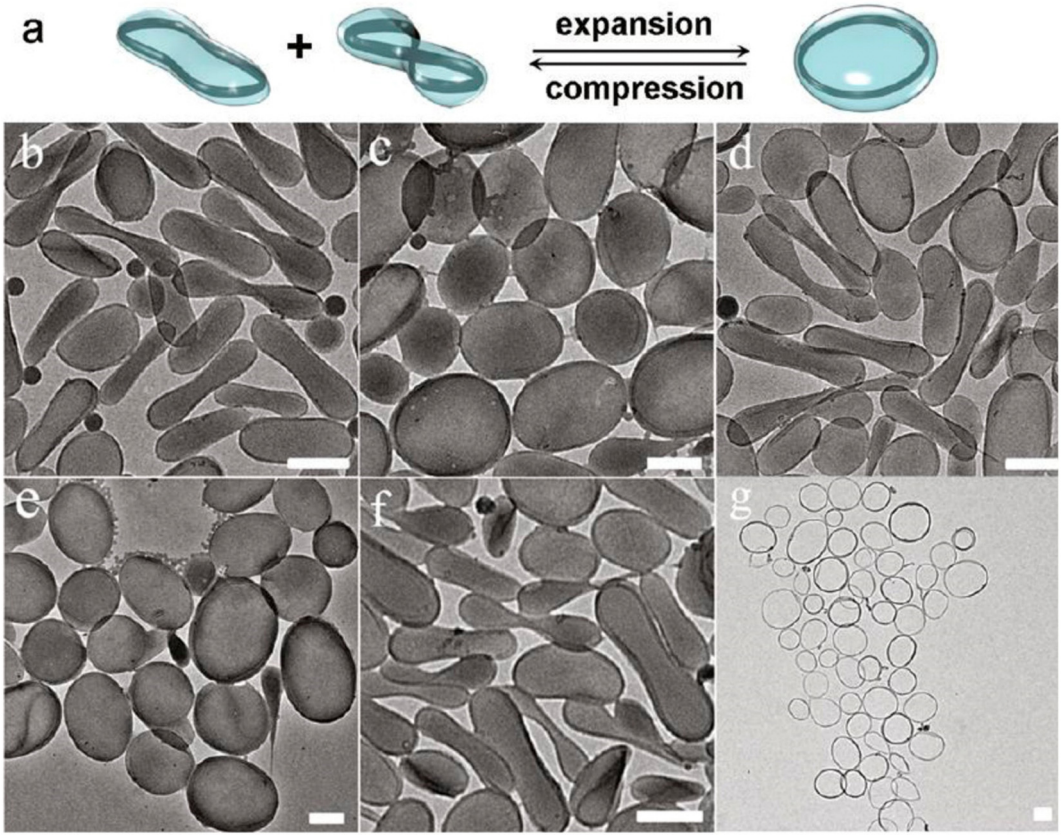

Fig. 15 Schematic Schematics illustration (a) and TEM images of CNT rings underwent several consecutive steps of structural transformation: compressed rings. (b) were expanded to circular rings (c) by moderate swelling of their shells, they were compressed again to (d), and then finally expanded by dissolving away their polymer shells (e)–(g). All scale bars are 200 nm reproduced with permission.[131] Copyright 2011, American Chemical Society.

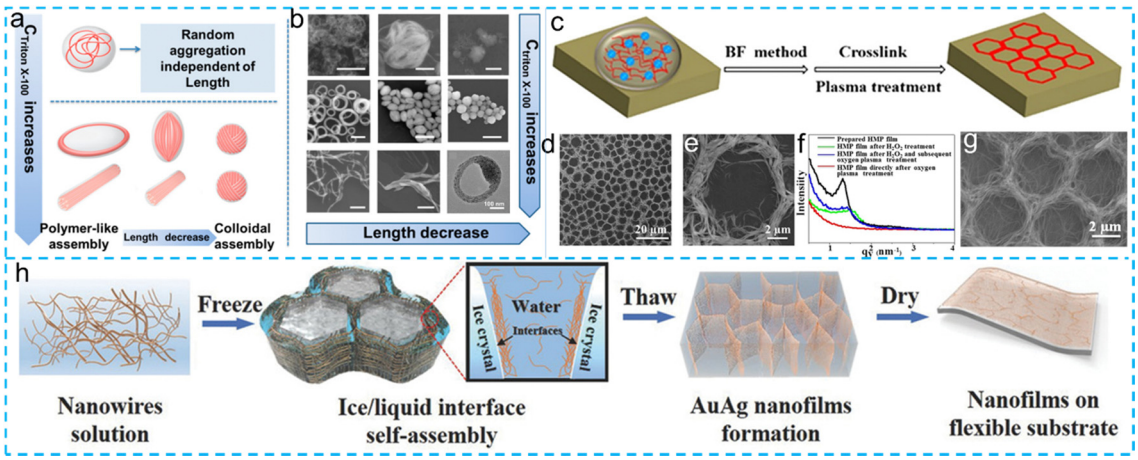

Fig. 16 (a) Schematic illustration of the assembly of ultrathin AuNWs in a solvent-shifting emulsion system. (b) SEM and TEM images of different AuNW-based assembly structures: Au nanorings, Au nanograins, Au superlattice nanospheres. Reproduced with permission.[133] Copyright 2017 American Chemical Society. (c) Schematic illustration of the HMP film prepared from ultrathin Au NW on Si substrate, (d) SEM image of HMP film after H_2O_2 treatment and oxygen plasma treatment, (e) high-magnification SEM image of panel a. The intensity distribution of the corresponding lines in panels is shown in panel (f). (g) high-resolution SEM image of the HMP film prepared from ultrathin Au NW on Si substrate. Reproduced with permission.[132] Copyright 2017 American Chemical Society. (h) Preparation of ultrathin AuAg nanofilms on the substrate by ice-templated assembly of ultrathin AuAg nanowires. Reproduced with permission.[134] 2018 WILEY-VCH Verlag GmbH & Co. KGaA, Weinheim.

detect radio frequency signals over a wide frequency range. When exciting the helical carbon nanotube windings either electrically or acoustically, a resonant response of the device was observed. The resonators are sensitive to mass changes as

small as a few tens of attograms, and they may play a major role in future nanoelectromechanical components.

The Wang group conducted *in situ* heating experiments on SiO_2 nanosprings using a focused beam in a transmission electron microscope (TEM). They observed that a segment of the nanospring could be expanded with heating.[32] This expansion was accompanied by a contraction of the nanospring near the junction with a straight wire, indicating that heating reduces the local spring constant. The corresponding expansion and contraction represent a redistribution of force along the nanospring to achieve equilibrium or a static mechanical condition. Subsequent electron beam heating of the contracted part led to expansion, supporting the idea that e-beam heating reduces the spring constant. Additionally, they demonstrated that SiO_2 nanosprings could be deflected with the tip of an atomic force microscope (AFM). However, they did not achieve quantitative measurements of the mechanical properties. In contrast, Rodney S. Ruoff and his colleagues successfully obtained a direct experimental measurement of the mechanical response of carbon nanocoils under tensile loading.[137] Carbon nanocoils were clamped between two AFM tips inside of a SEM, and loaded in tension to a maximum relative elongation of 42%. The deformation of nanocoil agrees well with an analytical model of the spring constant that accounts for the geometric nonlinearity. Quantitatively, from the load *versus* elongation data (determined from the acquired SEM images), the spring constant (K) values were fixed. The nanocoil behaves like an elastic spring with spring constant K of 0.12 N m^{-1} in the low-strain regime.

Similarly, the mechanical response of a multiwalled carbon nanospring under compression was examined with an AFM.[138] Cantilever deflection, oscillation amplitude, and resonance were simultaneously monitored during the cycled movement of the scanner. A nonlinear response of the nanospring was observed, consistent with compression and buckling of the nanospring. Wang group studied the super elasticity and nanoscale fracture behaviour of the ZnO superlattice nanosprings.[47,139] *Via in situ* manipulation using the nanoprobe tip inside a focused ion beam microscope (FIB) or AFM tip, the ZnO nanospring could elastically recover it shapes without obvious plastic deformation after extremely compression or stretching, showed excellent super elasticity (shape memory), which is certainly not possible with traditional steel springs. The spring constant of was found to be $\sim$4 N m^{-1} at a low strain regime,[47] and it could be increased continuously up to 300–800% upon experimental maximum extension.[139] As a new category of shape memory nanostructures made of ceramics, the superlattice-structured ZnO nanospring may be a potential application in nanoscale energy storage, buffer, indicator, and transducer, micro-electromechanical system (MEMS), nanoelectromechanical systems (NEMS), and can be made into smart micro nanoantessas possibly with large bandwidths.

The helical nanosprings, which were prepared by controlled self-rolling of strained films, also showed excellent mechanical strength *via* the micromanipulation technique.[74,76–79] The as-prepared rolled-up nanospring, which rolled from an 11 nm SiGe/8 nm Si/21 nm Cr multilayer, was cut off from substrate by a micromanipulation with a W tip (Fig. 17(a)–(c)), and then placed between AFM cantilever and the W tip within a SEM. By moving the W tip the nanosprings could be expanded and compressed. The applied force could be measured by the AFM cantilever and the deformation of nanospring was

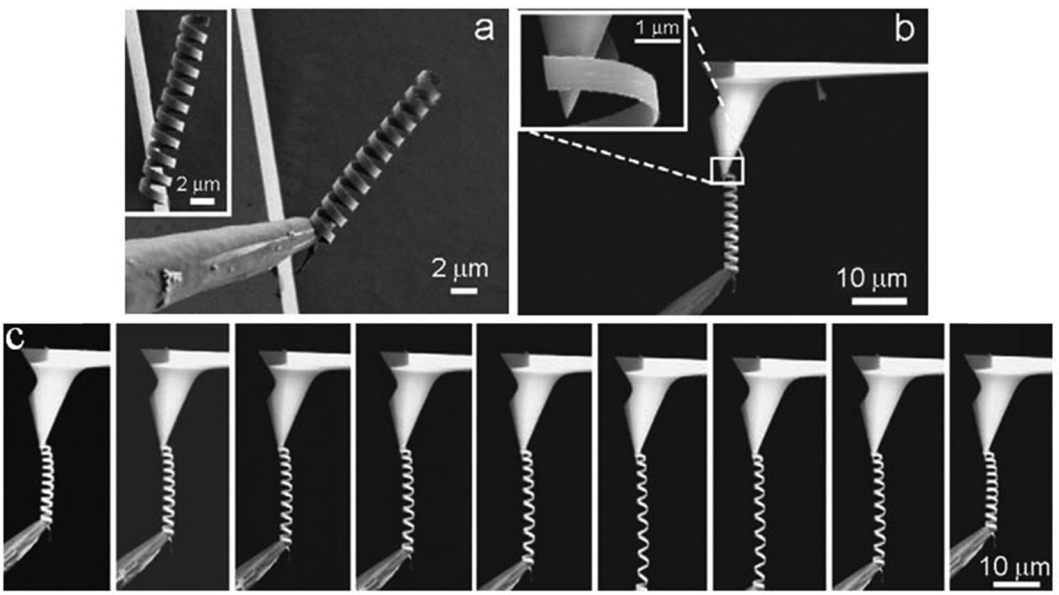

Fig. 17 SEM images for pick-up and manipulation process of SiGe/Si/Cr nanosprings, (a) pick up a as-fabricated nanospring into a W tip, and (b) place it between the W tip and AFM cantilever, the nanospring was fixed to AFM cantilever by soldering using electron beam-induced position. (c) Stretching and relaxing the nanospring between W tip and the AFM cantilever for stiffness characterization (from left to right). Reproduced with permission.[140] Copyright 2007 Elsevier Ltd. All rights reserved.

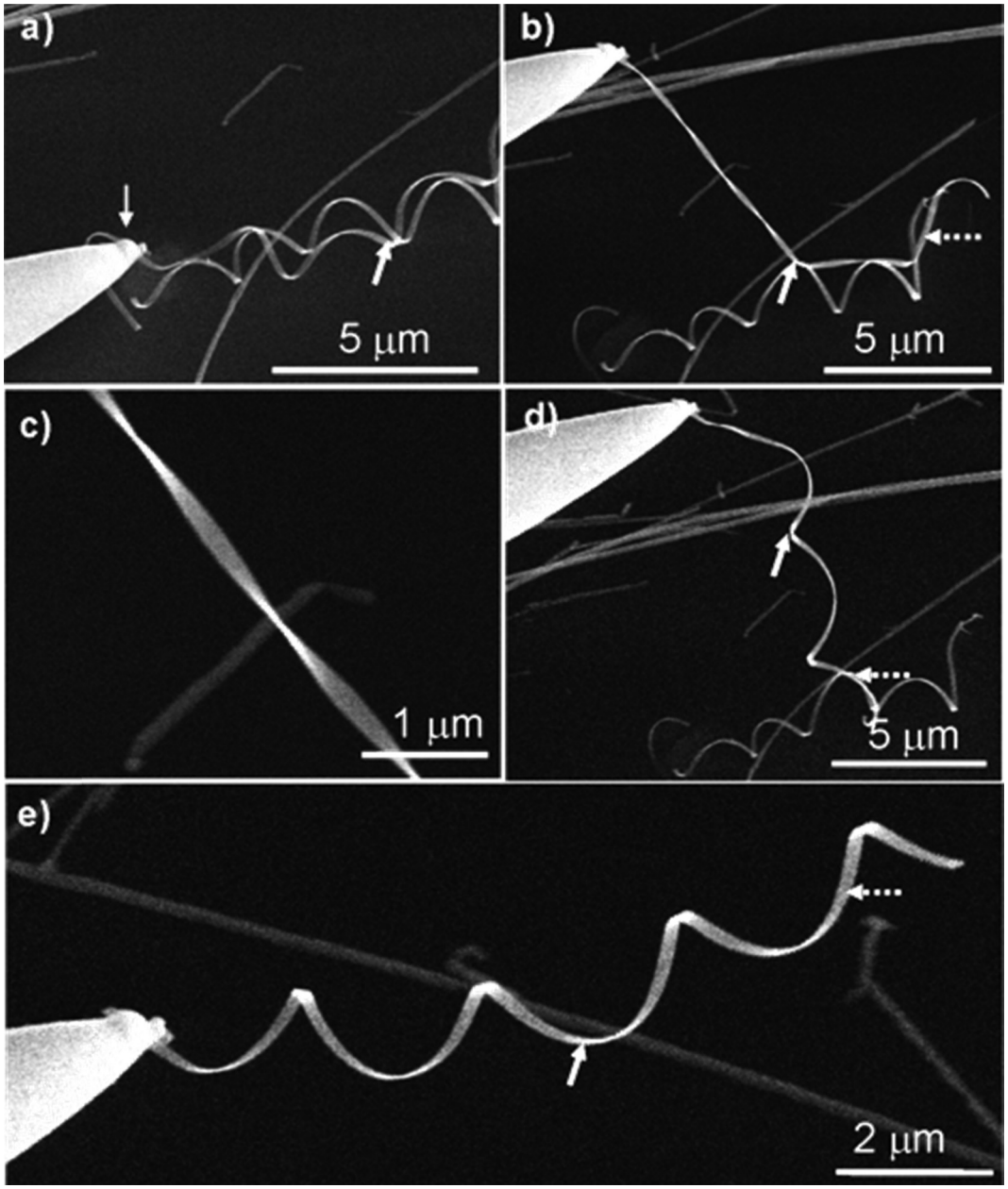

Fig. 18 SEM images showed the manipulation process of a ZnO helical nanospring deposited on Si substrate upon extremely large axial stretching and shape-recovery process. (a) One end of a nanohelix was welded with Pt onto a tungsten nanoprobe. (b) An attempt to extract the welded nanohelix out of the entangled nanohelices. (c) An enlarged SEM image showing the extremely stretched nanohelix. (d) Continued extraction led to an initial release of the welded nanohelix from the entangled point and a recovery of the nanohelix shape. (e) A complete restoring of the nanohelix shape after the manipulation in b and c, suggests a super elasticity (shape memory) behaviour. Reproduced with permission.[142] Copyright 2006, American Chemical Society.

visualized by SEM.[140] Fig. 18(a)–(e) shows a manipulation process of stretching and relaxing nanosprings. The durability of nanospring was measured by loading and unloading tension for several cycles, and no obvious deformation was observed. The nanosping showed excellent elasticity that a linear dependence between applied force and extension was found until the spring was extended to 91% of its origin length. The spring constant here is 0.003 N m^{-1}, which is much lower than carbon and ZnO naospring.[79] Such nanspring can be a potential application as ultra-sensitive force sensors. Coiled nanosprings also show promising mechanical properties at the nanoscale. *In situ* experimental configuration for studying the mechanical deformation of a CNT ring, which is formed by folding a long and thin SWNT bundle.[141] The CNT ring is horizontally fixed to a probe, and then was pushed (or pulled away from) against a vertically placed substrate by an external force *P*. The CNT ring displayed excellent elastic behaviour during the compression and tension process.[142]

In addition to employing nanomanipulators and nanomechanical testing, our research group has developed a solution-based approach to showcase the storage and release of mechanical energy at the nanoscale using nanosprings. In our system, Au nanowires coil into nanosprings driven by the energy minimization of the combined AuNW–polymer composites.[91,96,143] As a PSPAA micelle lowers its surface energy through contraction, the strain energy in the AuNW increases as its outer surface stretches in tension while the inner surface compresses. Consequently, the strained energy is stored in coiled nanosprings confined within the polymer shell. This stored energy is released by swelling or removing the polymer shell, causing the coiled Au nanospring to spontaneously spring back to nearly straight wires, releasing internal stress. Some kinks observed in the nanowire may result from uneven swelling and the release of mechanical energy onto a few spots, causing inelastic deformations of AuNWs. However, the fusion and inelastic buckling of ultrathin AuNWs make the coiling–uncoiling process challenging to reverse.

To overcome this drawback, we have further developed carbon nanosprings using a similar method to gold nanosprings. Due to strong interactions among their loops, coiled carbon nanosprings do not spontaneously uncoil when the polymer shells are swelled or removed, maintaining a coiled ring structure. These coiled rings exhibit reversible structural transformations in a colloidal solution and can mimic the reversible elastic motions of typical macroscopic rings. While the elastic motion of nano-objects has been studied using rings and helical nanostructures, most prior reports were based on manipulating individual nanostructures. This method introduces a new strategy for manipulating an entire population of CNT rings in a colloidal solution. The indirect shape control means that one does not have to manipulate each nanostructure individually, requiring perfect dexterity and spatial resolution.

2.7. Simulation and machine learning in nanospring study

Integrating simulation techniques like molecular dynamics and finite element modelling with machine learning is paramount in advancing nanospring study. Focusing on machine learning's role in design and optimization, alongside bridging multi-scale modelling approaches, promises to unlock new insights and innovations in this field.

In materials science, microscopy serves as the primary method for structural characterization, yet its manual analysis poses challenges. As interest grows in automating this process using machine learning, a hurdle emerges: traditional training necessitates vast labelled image datasets, prone to human error. To address this, a semi-supervised transfer learning method was proposed as shown in Fig. 19(a).[144] A small set of labelled microscopy images was used for training, leveraging self-supervised learning techniques for feature extraction. Specifically, SimCLR and Barlow-Twins were applied on transmission electron microscopy (TEM) images. This approach enables automated classification of nanowire morphologies and segmentation tasks, crucial for quantifying domain sizes and shape analysis. Utilizing synthetic images resembling experimental ones, a study trained Mask region-based CNNs for segmenting vanadium pentoxide nanowires in optical density-based Spectro microscopy images.[145] Fig. 19(b) illustrates the process. The model showcased remarkable instance segmentation capabilities on complex nanowires, yielding reliable statistical data. This approach hints at broader applicability, even for segmenting nanowires in scanning electron microscopy images, distinct from its training set. Additionally, a novel two-step framework integrates Gaussian process-based Bayesian optimization (BO) and a deep neural network (DNN) to swiftly synthesize silver nanoparticles with tailored absorbance spectra.[146] Illustrated in Fig. 19(c), this method converges to the target spectrum after just 120 samplings. The DNN, trained on a sizable dataset, forecasts the achievable color palette, ensuring human interpretability. This efficient approach optimizes nanomaterial synthesis while unravelling crucial insights into the chemical-optical correlation. Going beyond the above, random forest algorithms employ bagging, combining multiple decision trees (DTs) to predict outcomes (Fig. 19(d)).[147] RF uses sample and property bagging, reducing properties and creating diverse DTs. Analyzing DT outcomes yields a final prediction, leveraging anticipated outcomes to refine property selection.

Recent attention in diverse fields, including materials science, has focused on machine-learning (ML) methods.[149] ML interatomic potentials (MLIPs) are particularly effective in assessing mechanical and structural properties of novel materials and nanostructures.[150] Trained on first-principles datasets, MLIPs match accuracy while offering flexibility for diverse compositions. They integrate seamlessly with common CMD approaches, enabling simulations of large systems and temperature effects.[151] MLIPs facilitate first-principles multiscale modelling, bridging accuracy levels to explore macroscopic system responses.[152,153] For example, researchers introduced a novel concept, first-principles multiscale modelling of mechanical properties (Fig. 19(e)), bridging *ab initio* accuracy to assess macroscopic systems.[148] Machine-learning interatomic potentials (MLIPs), tailored to *ab initio* data, are integral to this approach. Demonstrated with graphene/borophene heterostructures, MLIPs excel over CMD models, evaluating properties at room temperature. MLIP-based CMD informs continuum models for heterostructures *via* finite element analysis.

3. Applications of nanosprings

The imperative development of wireless nanodevices spans the sensing, medical, defense, and personal electronics realms. Vital for implanted biomedical devices is self-powering sans batteries. Exploring nanotechnologies becomes crucial for converting mechanical (*e.g.*, body movement), vibrational (*e.g.*, acoustic waves), and hydraulic (*e.g.*, body fluid flow) energies into electrical power. This innovation ensures nanodevice functionality without reliance on traditional power sources, enhancing versatility and sustainability across various applications in modern technology landscapes.

Recent advancements in chemical vapor deposition enabled the production of high-quality single-layer $MoSi_2N_4$

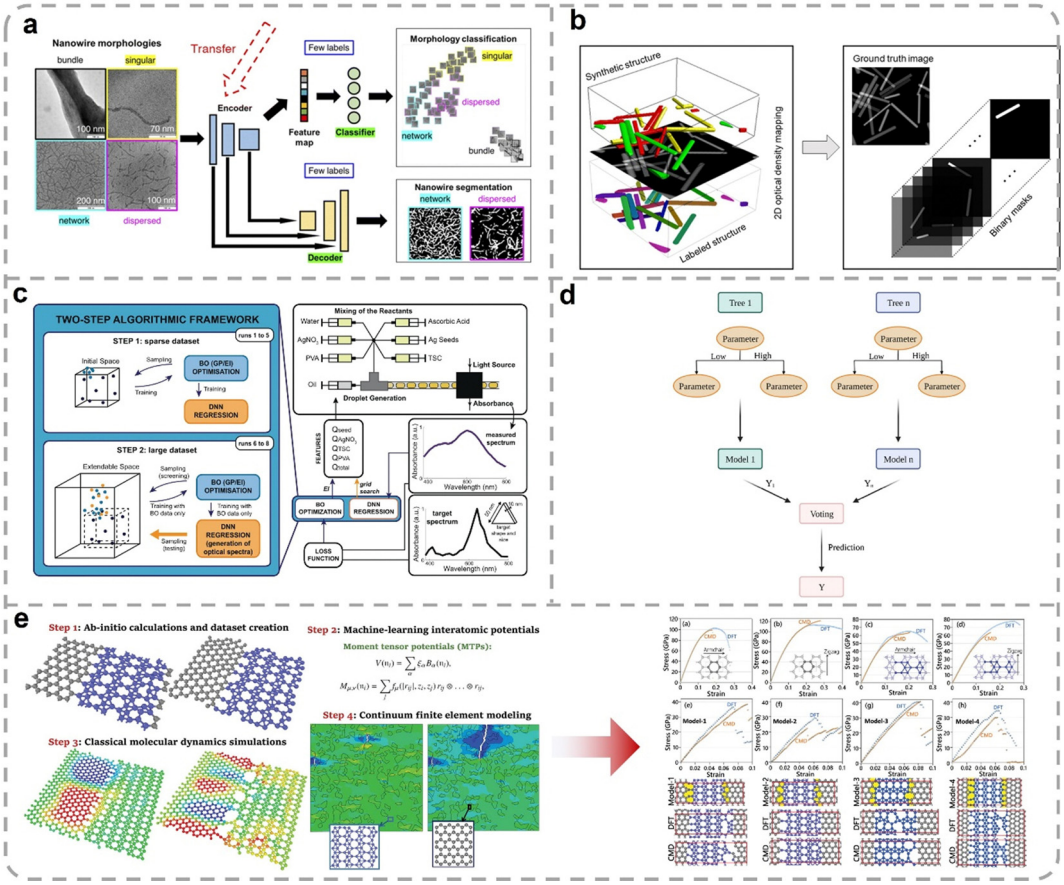

Fig. 19 (a) Two-step generalized semi-supervised machine learning workflow for classification and segmentation of microscopy images. Reproduced with permission.[144] Copyright 2022, Royal Society of Chemistry. (b) Synthetically generated dataset for training, where 3D microstructures are compressed into optical density-based images as input data, and individually labelled nanowires create binary masks for output data. Reproduced with permission. Reproduced with permission.[145] Copyright 2022, The Author(s). (c) Algorithmic framework for a high-throughput experimental loop, featuring a two-step optimization process with BO and DNN sampling and validating parameter space, tested on a droplet-based microfluidic platform. Reproduced with permission.[146] Copyright 2021, The Author(s). (d) An example of a random forest algorithm for AgNW polyol synthesis, using bagging to generate multiple decision tree outcomes for statistical prediction analysis. Reproduced with permission.[147] Copyright 2023, King Abdulaziz City for Science and Technology. (e) Proposed first-principles multiscale modelling strategy to simulate the mechanical and failure response of graphene/borophene coplanar heterostructures. Reproduced with permission.[148] Copyright 2021 The Authors. Advanced Materials published by Wiley-VCH GmbH.

at centimetre scales.[154] Inspired by this, researchers conducted extensive first-principles simulations on MA_2Z_4 monolayers (M = Cr, Mo, W; A = Si, Ge; Z = N, P) (Fig. 20(a)).[155] These nanosheets exhibit dynamical stability, exceptional mechanical properties, and diverse electronic features, ranging from antiferromagnetic metal to semiconductors (Fig. 20(b)–(d)). Notably, $MoSi_2N_4$ and WSi_2N_4 monolayers demonstrate promising characteristics for optoelectronic and photocatalytic applications.

Developing wireless nanodevices is crucial across sensing, medical science, defence, and personal electronics, especially for self-powered implanted biomedical devices. Nanotechnologies are pivotal for converting mechanical, vibrational, and hydraulic energy into electrical power, a vital stride towards self-sustaining nanosystems.[159–161]

Researchers innovatively harness piezoelectric zinc oxide nanowire arrays to convert mechanical energy into electricity, exploiting ZnO's piezoelectric and semiconducting properties, and Schottky barrier gating effects.[157] This approach has led to the development of DC nanogenerators driven by ultrasonic waves in biofluid and textile-fiber-based generators for harvesting low-frequency mechanical energy (Fig. 20(e)). Gold nanohelices in a three-dimensional array efficiently polarize light across various wavelengths.[162]

Scientists scrutinized light propagation in a uniaxial photonic metamaterial, featuring three-dimensional gold helices on a two-dimensional square lattice (Fig. 20(f)).[158] Fabrication involves direct laser writing into positive-tone photoresist and subsequent electrochemical deposition of gold. For light traveling along the helix axis, the structure selectively blocks circular polarization matching its handedness, while transmitting the opposite, across a frequency range surpassing one octave. This scalable design serves as a compact, broadband circular polarizer.[163,164]

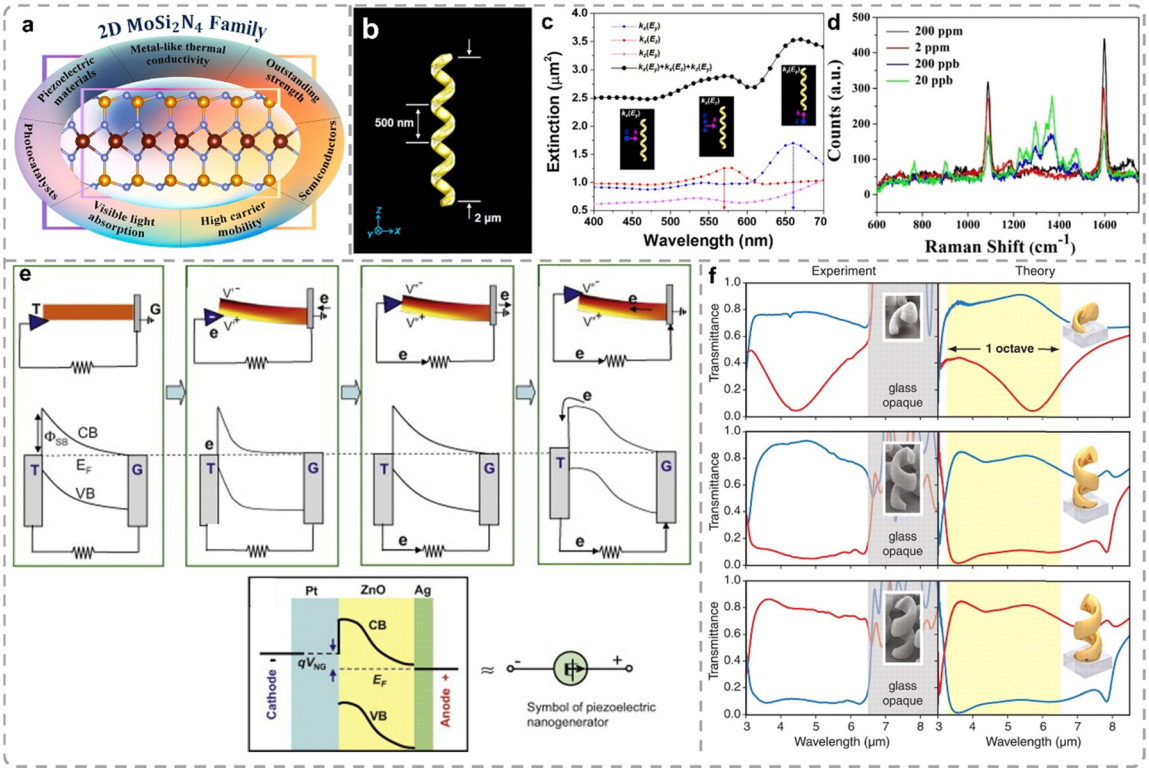

Fig. 20 (a) Recent advancements in chemical vapor deposition have enabled the fabrication of centimetre-scale high-quality single-layer $MoSi_2N_4$. Reproduced with permission.[155] Copyright 2020 Elsevier Ltd. All rights reserved. (b) Schemes of AuNHs for FDTD simulations: side views showing dimensions and simulation system coordination and (c) Wavelength-dependent extinction cross-section of AuNHs with different light incidences. (d) SERS spectra of AuNHs using 4-MBA as the probe. Reproduced with permission.[156] Copyright 2020 American Chemical Society. (e) Schematic of a NW with a grounded end and a conductive AFM tip shows how deflection changes the conduction band profile, causing electron flow. Reproduced with permission.[157] Copyright 2008 WILEY-VCH Verlag GmbH & Co. KGaA, Weinheim. (f) Measured and calculated normal-incidence transmittance spectra for LCP (red) and RCP (blue) helices with varying pitches. Reproduced with permission.[158] Copyright 2009, the American Association for the Advancement of Science.

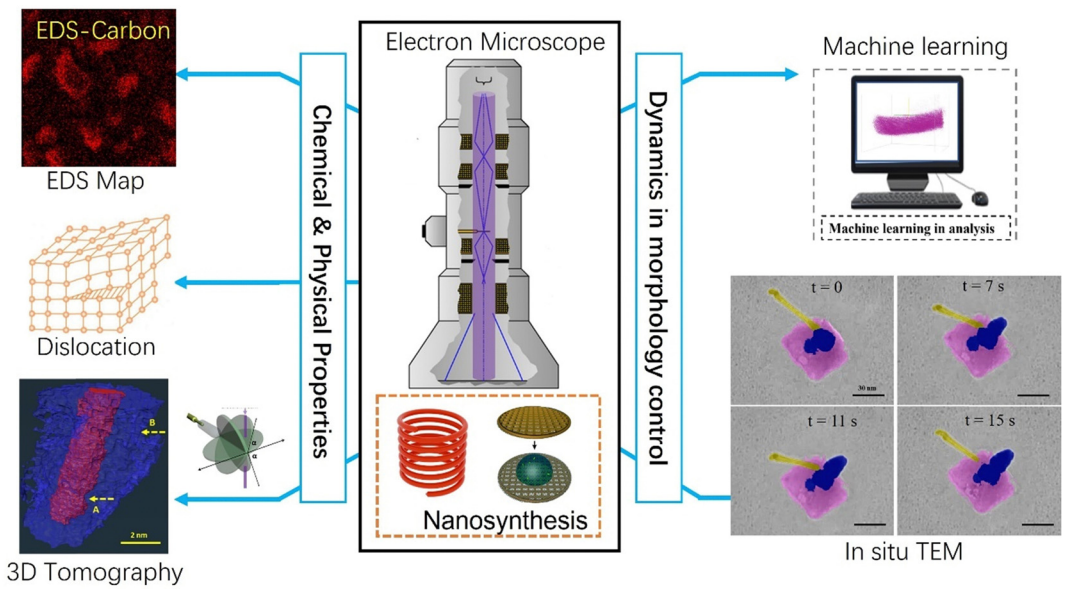

Fig. 21 The combination of characterization tools to study the growth mechanism of nanosprings. Note: experimental data shown is reproduced with permission.[172,173] Copyright 2022 Wiley-VCH GmbH.

4. Conclusions and perspectives

Advancements in materials science are pushing the boundaries of nanospring morphology control, thanks to progress in molecular engineering, surface ligand chemistry, nanosynthesis techniques, and state-of-the-art characterization tools, including *in situ* transmission electron microscopy (TEM), TEM 3D tomography, and machine learning (Fig. 21). Meticulous molecular engineering empowers researchers to customize the surface chemistry and ligand interactions of nanomaterials, influencing their self-assembly and eventual morphology.[165–167] This precise control facilitates the synthesis of nanosprings with tailored properties and functionalities. Furthermore, advancements in nanosynthesis techniques offer the capability to finely manipulate the size, shape, and composition of nanosprings,[168–171] thereby expanding the design possibilities for materials with distinct and unique properties.

The incorporation of *in situ* transmission electron microscopy (TEM) techniques allows for the real-time observation of nanospring formation and evolution at the nanoscale. This capability provides unprecedented insights into the underlying mechanisms governing their morphology and growth dynamics.[174–181] Furthermore, TEM 3D tomography offers detailed three-dimensional reconstructions of nanospring structures, enabling comprehensive characterization and structural analysis with nanoscale resolution.[182–186]

To summarize, this feature reviews recent advancements in the successful fabrication of nanosprings, with a particular emphasis on morphology control and mechanical properties. Vapor phase synthesis achieves nanospring formation through an induced anisotropic growth mechanism. Template methods produce helical nanosprings either from hard springlike templates or through the formation of helical structures with organic molecules. Post-treatment methods combine one-dimensional synthesis processing with force-induced bending or coiling to induce the assembly of one-dimensional nanowires/nanobelts into three-dimensional nanosprings. While the vapor phase methodology has drawbacks, such as the need for high temperatures and specific equipment, limiting its broad application due to high fabrication costs and scalability issues, as well as the inability to produce metallic springs, templating methodologies have demonstrated impressive examples of nanosprings. Many of these examples cannot be achieved through directed growth processes. However, a common trait in most cases is related to adsorption and deposition processes. Additionally, the molecular engineering of crystal surfaces could be developed to control nanospring morphology at the nanoscale. It is believed that, with the advancement of nanoscience and nanotechnology, nanospring morphology control and characterization, driven by molecular engineering, surface ligand chemistry, nanosynthesis, *in situ* TEM, TEM 3D tomography, and machine learning, offer precise manipulation, real-time observation, and comprehensive analysis. This advancement is poised to propel materials science forward and foster innovation across diverse applications.[171,177,187,188]

Note

There are no ethical concerns in this review.

Author contributions

D. Yang and R. Huang: conceptualization, information collection, writing (original draft and editing). B, Zou, R. Wang, and Y. Wang: information collection, writing (original draft). E. H. Ang and X. Song: conceptualization, writing (editing), supervision, project administration.

Data availability

No primary research results, software or code have been included and no new data were generated or analysed as part of this review.

Conflicts of interest

There are no conflicts of interest to declare.

Acknowledgements

This work was supported by the starting-up funding of Hefei University of Technology under grant no. 13020-03712021026 and the National Institution of Education Start-Up Grant (NIE-SUG4/20AHX).

References

1 B. A. Korgel, Nanosprings take shape, *Science*, 2005, **309**(5741), 1683–1684.
2 A. Cho, Nanotechnology – Pretty as you please, curling films turn themselves into nanodevices, *Science*, 2006, **313**(5784), 164–165.
3 S. W. Chung, D. S. Ginger, M. W. Morales, Z. F. Zhang, V. Chandrasekhar, M. A. Ratner and C. A. Mirkin, Top-down meets bottom-up: Dip-pen nanolithography and DNA-directed assembly of nanoscale electrical circuits, *Small*, 2005, **1**(1), 64–69.
4 Y. Zhao, L. N. An and J. Y. Fang, Buckling of lipid tubules in shrinking liquid droplets, *Nano Lett.*, 2007, **7**(5), 1360–1363.
5 A. E. Cohen and L. Mahadevan, Kinks, rings, and rackets in filamentous structures, *Proc. Natl. Acad. Sci. U. S. A.*, 2003, **100**(21), 12141–12146.
6 R. T. K. Baker, P. S. Harris and S. Terry, Unique form of filamentous carbon, *Nature*, 1975, **253**(5486), 37–39.
7 S. Amelinckx, X. B. Zhang, D. Bernaerts, X. F. Zhang, V. Ivanov and J. B. Nagy, A formation mechanism for catalytically grown helix-shaped graphite nanotubes, *Science*, 1994, **265**(5172), 635–639.
8 L. J. Pan, M. Zhang and Y. Nakayama, Growth mechanism of carbon nanocoils, *J. Appl. Phys.*, 2002, **91**(12), 10058–10061.

9 T. Luo, J. W. Liu, L. Y. Chen, S. Y. Zeng and Y. T. Qian, Synthesis of helically coiled carbon nanotubes by reducing ethyl ether with metallic zinc, *Carbon*, 2005, **43**(4), 755–759.
10 M. Lu, H. L. Li and K. T. Lau, Formation and growth mechanism of dissimilar coiled carbon nanotubes by reduced-pressure catalytic chemical vapor deposition, *J. Phys. Chem. B*, 2004, **108**(20), 6186–6192.
11 V. Bajpai, L. Dai and T. Ohashi, Large-scale synthesis of perpendicularly aligned helical carbon nanotubes, *J. Am. Chem. Soc.*, 2004, **126**(16), 5070–5071.
12 H. Q. Hou, Z. Jun, F. Weller and A. Greiner, Large-scale synthesis and characterization of helically coiled carbon nanotubes by use of Fe(CO)(5) as floating catalyst precursor, *Chem. Mater.*, 2003, **15**(16), 3170–3175.
13 S. M. Huang, A. W. H. Mau, T. W. Turney, P. A. White and L. M. Dai, Patterned growth of well-aligned carbon nanotubes: A soft-lithographic approach, *J. Phys. Chem. B*, 2000, **104**(10), 2193–2196.
14 L. M. Dai and A. W. H. Mau, Controlled synthesis and modification of carbon nanotubes and C-60: Carbon nanostructures for advanced polymer composite materials, *Adv. Mater.*, 2001, **13**(12–13), 899–913.
15 V. Bajpai, L. M. Dai and T. Ohashi, Large-scale synthesis of perpendicularly aligned helical carbon nanotubes, *J. Am. Chem. Soc.*, 2004, **126**(16), 5070–5071.
16 Q. Zhang, M. Q. Zhao, D. M. Tang, F. Li, J. Q. Huang, B. L. Liu, W. C. Zhu, Y. H. Zhang and F. Wei, Carbon-Nanotube-Array Double Helices, *Angew. Chem., Int. Ed.*, 2010, **49**(21), 3642–3645.
17 H. Hou, Z. Jun, F. Weller and A. Greiner, Large-scale synthesis and characterization of helically coiled carbon nanotubes by use of Fe (CO) 5 as floating catalyst precursor, *Chem. Mater.*, 2003, **15**(16), 3170–3175.
18 B. K. Gupta, V. Shanker, M. Arora and D. Haranath, Photoluminescence and electron paramagnetic resonance studies of springlike carbon nanofibers, *Appl. Phys. Lett.*, 2009, **95**(7), 073115.
19 R. P. Gao, Z. L. Wang and S. S. Fan, Kinetically controlled growth of helical and zigzag shapes of carbon nanotubes, *J. Phys. Chem. B*, 2000, **104**(6), 1227–1234.
20 S. Motojima and Q. Q. Chen, Three-dimensional growth mechanism of cosmo-mimetic carbon microcoils obtained by chemical vapor deposition, *J. Appl. Phys.*, 1999, **85**(7), 3919–3921.
21 S. Motojima, S. Asakura, T. Kasemura, S. Takeuchi and H. Iwanaga, Catalytic effects of metal carbides, oxides and Ni single crystal on the vapor growth of micro-coiled carbon fibers, *Carbon*, 1996, **34**(3), 289–296.
22 K. Hernadi, L. Thien-Nga and L. Forro, Growth and microstructure of catalytically produced coiled carbon nanotubes, *J. Phys. Chem. B*, 2001, **105**(50), 12464–12468.
23 Y. Qin, Z. K. Zhang and Z. L. Cui, Helical carbon nanofibers with a symmetric growth mode, *Carbon*, 2004, **42**(10), 1917–1922.
24 N. J. Tang, J. F. Wen, Y. Zhang, F. X. Liu, K. J. Lin and Y. W. Du, Helical Carbon Nanotubes: Catalytic Particle Size-Dependent Growth and Magnetic Properties, *ACS Nano*, 2010, **4**(1), 241–250.
25 W. Wang, K. Q. Yang, J. Gaillard, P. R. Bandaru and A. M. Rao, Rational synthesis of helically coiled carbon nanowires and nanotubes through the use of tin and indium catalysts, *Adv. Mater.*, 2008, **20**(1), 179–182.
26 P. R. Bandaru, C. Daraio, K. Yang and A. M. Rao, A plausible mechanism for the evolution of helical forms in nanostructure growth, *J. Appl. Phys.*, 2007, **101**(9), 094307.
27 W. C. Liu, H. K. Lin, Y. L. Chen, C. Y. Lee and H. T. Chiu, Growth of Carbon Nanocoils from K and Ag Cooperative Bicatalyst Assisted Thermal Decomposition of Acetylene, *ACS Nano*, 2010, **4**(7), 4149–4157.
28 J. N. Wang, L. F. Su and Z. P. Wu, Growth of highly compressed and regular coiled carbon nanotubes by a spray-pyrolysis method, *Cryst. Growth Des.*, 2008, **8**(5), 1741–1747.
29 D. Yu, J. Q. Wu, Q. Gu and H. K. Park, Germanium telluride nanowires and nanohelices with memory-switching behavior, *J. Am. Chem. Soc.*, 2006, **128**(25), 8148–8149.
30 D. N. McIlroy, D. Zhang, Y. Kranov and M. G. Norton, Nanosprings, *Appl. Phys. Lett.*, 2001, **79**(10), 1540–1542.
31 D. Q. Zhang, A. Alkhateeb, H. M. Han, H. Mahmood, D. N. McIlroy and M. G. Norton, Silicon carbide nanosprings, *Nano Lett.*, 2003, **3**(7), 983–987.
32 H. F. Zhang, C. M. Wang, E. C. Buck and L. S. Wang, Synthesis, characterization, and manipulation of helical SiO_2 nanosprings, *Nano Lett.*, 2003, **3**(5), 577–580.
33 M. Nath and B. A. Parkinson, Superconducting MgB_2 nanohelices grown on various substrates, *J. Am. Chem. Soc.*, 2007, **129**(37), 11302–11303.
34 D. McIlroy, D. Zhang, Y. Kranov and M. G. Norton, Nanosprings, *Appl. Phys. Lett.*, 2001, **79**(10), 1540–1542.
35 H. F. Zhang, C. M. Wang and L. S. Wang, Helical crystalline SiC/SiO_2 core–shell nanowires, *Nano Lett.*, 2002, **2**(9), 941–944.
36 Z. Y. Zhang, X. L. Wu, L. L. Xu, J. C. Shen, G. G. Siu and P. K. Chu, Synthesis, growth mechanism, and light-emission properties of twisted SiO_2 nanobelts and nanosprings, *J. Chem. Phys.*, 2008, **129**(16), 164702.
37 J. H. Zhan, Y. Bando, J. Q. Hu, F. F. Xu and D. Golberg, Unconventional gallium oxide nanowires, *Small*, 2005, **1**(8–9), 883–888.
38 M. J. Bierman, Y. K. A. Lau, A. V. Kvit, A. L. Schmitt and S. Jin, Dislocation-driven nanowire growth and Eshelby twist, *Science*, 2008, **320**(5879), 1060–1063.
39 Y. K. A. Lau, D. J. Chernak, M. J. Bierman and S. Jin, Formation of PbS Nanowire Pine Trees Driven by Screw Dislocations, *J. Am. Chem. Soc.*, 2009, **131**(45), 16461–16471.
40 J. Zhu, H. L. Peng, A. F. Marshall, D. M. Barnett, W. D. Nix and Y. Cui, Formation of chiral branched nanowires by the Eshelby Twist, *Nat. Nanotechnol.*, 2008, **3**(8), 477–481.

41 M. J. Bierman, Y. A. Lau, A. V. Kvit, A. L. Schmitt and S. Jin, Dislocation-driven nanowire growth and Eshelby twist, *Science*, 2008, **320**(5879), 1060–1063.
42 J. D. Eshelby, Screw dislocations in thin rods, *J. Appl. Phys.*, 1953, **24**(2), 176–179.
43 Y. A. Lau, D. J. Chernak, M. J. Bierman and S. Jin, Formation of PbS nanowire pine trees driven by screw dislocations, *J. Am. Chem. Soc.*, 2009, **131**(45), 16461–16471.
44 X. Y. Kong and Z. L. Wang, Spontaneous polarization-induced nanohelixes, nanosprings, and nanorings of piezoelectric nanobelts, *Nano Lett.*, 2003, **3**(12), 1625–1631.
45 P. X. Gao, Y. Ding, W. Mai, W. L. Hughes, C. Lao and Z. L. Wang, Conversion of zinc oxide nanobelts into superlattice-structured nanohelices, *Science*, 2005, **309**(5741), 1700–1704.
46 W. L. Hughes and Z. L. Wang, Formation of piezoelectric single-crystal nanorings and nanobows, *J. Am. Chem. Soc.*, 2004, **126**(21), 6703–6709.
47 P. X. Gao, Y. Ding, W. J. Mai, W. L. Hughes, C. S. Lao and Z. L. Wang, Conversion of zinc oxide nanobelts into superlattice-structured nanohelices, *Science*, 2005, **309**(5741), 1700–1704.
48 R. S. Yang and Z. L. Wang, Springs, rings, and spirals of rutile-structured tin oxide nanobelts, *J. Am. Chem. Soc.*, 2006, **128**(5), 1466–1467.
49 G. Z. Shen, Y. Bando, C. Y. Zhi, X. L. Yuan, T. Sekiguchi and D. Golberg, Single-crystalline cubic structured InP nanosprings, *Appl. Phys. Lett.*, 2006, **88**, 243106.
50 Y. Qin, Z. K. Zhang and Z. L. Cui, Helical carbon nanofibers prepared by pyrolysis of acetylene with a catalyst derived from the decomposition of copper tartrate, *Carbon*, 2003, **41**(15), 3072–3074.
51 H. Ogihara, M. Sadakane, Y. Nodasaka and W. Ueda, Shape-controlled synthesis of ZrO_2, Al_2O_3, and SiO_2 nanotubes using carbon nanofibers as templates, *Chem. Mater.*, 2006, **18**(21), 4981–4983.
52 G. W. Xie, Z. B. Wang, Z. L. Cui and Y. L. Shi, Ni–Fe–Co–P coatings on coiled carbon nanofibers, *Carbon*, 2005, **43**(15), 3181–3183.
53 Y. Qin, Y. Kim, L. B. Zhang, S. M. Lee, R. B. Yang, A. L. Pan, K. Mathwig, M. Alexe, U. Gosele and M. Knez, Preparation and Elastic Properties of Helical Nanotubes Obtained by Atomic Layer Deposition with Carbon Nanocoils as Templates, *Small*, 2010, **6**(8), 910–914.
54 Y. Wu, T. Livneh, Y. X. Zhang, G. Cheng, J. Wang, J. Tang, M. Moskovits and G. D. Stucky, Templated synthesis of highly ordered mesostructured nanowires and nanowire arrays, *Nano Lett.*, 2004, **4**(12), 2337–2342.
55 Y. Y. Wu, G. S. Cheng, K. Katsov, S. W. Sides, J. F. Wang, J. Tang, G. H. Fredrickson, M. Moskovits and G. D. Stucky, Composite mesostructures by nano-confinement, *Nat. Mater.*, 2004, **3**(11), 816–822.
56 Y. Y. Wu, T. Livneh, Y. X. Zhang, G. S. Cheng, J. F. Wang, J. Tang, M. Moskovits and G. D. Stucky, Templated synthesis of highly ordered mesostructured nanowires and nanowire arrays, *Nano Lett.*, 2004, **4**(12), 2337–2342.
57 W.-H. Tseng, C.-K. Chen, Y.-W. Chiang, R.-M. Ho, S. Akasaka and H. Hasegawa, Helical nanocomposites from chiral block copolymer templates, *J. Am. Chem. Soc.*, 2009, **131**(4), 1356–1357.
58 R. M. Ho, Y. W. Chiang, C. C. Tsai, C. C. Lin, B. T. Ko and B. H. Huang, Three-dimensionally packed nanohelical phase in chiral block copolymers, *J. Am. Chem. Soc.*, 2004, **126**(9), 2704–2705.
59 Y. W. Chiang, R. M. Ho, B. T. Ko and C. C. Lin, Springlike nanohelical structures in chiral block copolymers, *Angew. Chem., Int. Ed.*, 2005, **44**(48), 7969–7972.
60 W. H. Tseng, C. K. Chen, Y. W. Chiang, R. M. Ho, S. Akasaka and H. Hasegawa, Helical Nanocomposites from Chiral Block Copolymer Templates, *J. Am. Chem. Soc.*, 2009, **131**(4), 1356–1357.
61 J. H. Jung, Y. Ono, K. Hanabusa and S. Shinkai, Creation of both right-handed and left-handed silica structures by sol-gel transcription of organogel fibers comprised of chiral diaminocyclohexane derivatives, *J. Am. Chem. Soc.*, 2000, **122**(20), 5008–5009.
62 J. H. Jung, Y. Ono and S. Shinkai, Sol-gel polycondensation in a cyclohexane-based organogel system in helical silica: Creation of both right- and left-handed silica structures by helical organogel fibers, *Chem. – Eur. J.*, 2000, **6**(24), 4552–4557.
63 S. Kobayashi, N. Hamasaki, M. Suzuki, M. Kimura, H. Shirai and K. Hanabusa, Preparation of helical transition-metal oxide tubes using organogelators as structure-directing agents, *J. Am. Chem. Soc.*, 2002, **124**(23), 6550–6551.
64 Y. Y. Lin, Y. Qiao, C. Gao, P. F. Tang, Y. Liu, Z. B. Li, Y. Yan and J. B. Huang, Tunable One-Dimensional Helical Nanostructures: From Supramolecular Self-Assemblies to Silica Nanomaterials, *Chem. Mater.*, 2010, **22**(24), 6711–6717.
65 Y. G. Yang, M. Suzuki, H. Fukui, H. Shirai and K. Hanabusa, Preparation of helical mesoporous silica and hybrid silica nanofibers using hydrogelator, *Chem. Mater.*, 2006, **18**(5), 1324–1329.
66 E. D. Sone, E. R. Zubarev and S. I. Stupp, Semiconductor nanohelices templated by supramolecular ribbons, *Angew. Chem., Int. Ed.*, 2002, **41**(10), 1705–1709.
67 Y. Qiao, Y. Y. Lin, Y. J. Wang, Z. Y. Yang, J. Liu, J. Zhou, Y. Yan and J. B. Huang, Metal-Driven Hierarchical Self-Assembled One-Dimensional Nanohelices, *Nano Lett.*, 2009, **9**(12), 4500–4504.
68 Y. Inoue, M. Uota, M. Uchigasaki, S. Nishi, T. Torikai, T. Watari and M. Yada, Helical ruthenium compound templated by 1-dodecanesulfonate assemblies and its conversion into helical ruthenium oxide and helical metallic ruthenium, *Chem. Mater.*, 2008, **20**(17), 5652–5656.
69 S. Yang, L. Z. Zhao, C. Z. Yu, X. F. Zhou, J. W. Tang, P. Yuan, D. Y. Chen and D. Y. Zhao, On the origin of helical mesostructures, *J. Am. Chem. Soc.*, 2006, **128**(32), 10460–10466.
70 Y. Han, L. Zhao and J. Y. Ying, Entropy-driven helical mesostructure formation with achiral cationic surfactant templates, *Adv. Mater.*, 2007, **19**(18), 2454–2459.

71 J. F. Ye, H. J. Zhang, R. Yang, X. G. Li and L. M. Qi, Morphology-Controlled Synthesis of SnO_2 Nanotubes by Using 1D Silica Mesostructures as Sacrificial Templates and Their Applications in Lithium-Ion Batteries, *Small*, 2010, **6**(2), 296–306.
72 D. J. Bell, Y. Sun, L. Zhang, L. X. Dong, B. J. Nelson and D. Grützmacher, Three-dimensional nanosprings for electromechanical sensors, *Sens. Actuators, A*, 2006, **130**, 54–61.
73 L. Zhang, E. Deckhardt, A. Weber, C. Schonenberger and D. Grutzmacher, Controllable fabrication of SiGe/Si and SiGe/Si/Cr helical nanobelts, *Nanotechnology*, 2005, **16**(6), 655–663.
74 G. Hwang, H. Hashimoto, D. J. Bell, L. X. Dong, B. J. Nelson and S. Schon, Piezoresistive InGaAs/GaAs Nanosprings with Metal Connectors, *Nano Lett.*, 2009, **9**(2), 554–561.
75 V. Luchnikov, O. Sydorenko and M. Stamm, Self-rolled polymer and composite polymer/metal micro- and nanotubes with patterned inner walls, *Adv. Mater.*, 2005, **17**(9), 1177–1182.
76 D. J. Bell, L. X. Dong, B. J. Nelson, M. Golling, L. Zhang and D. Grutzmacher, Fabrication and characterization of three-dimensional InGaAs/GaAs nanosprings, *Nano Lett.*, 2006, **6**(4), 725–729.
77 D. J. Bell, Y. Sun, L. Zhang, L. X. Dong, B. J. Nelson and D. Grutzmacher, Three-dimensional nanosprings for electromechanical sensors, *Sens. Actuators, A*, 2006, **130**, 54–61.
78 D. Gruetzmacher, L. Zhang, L. Dong, D. Bell, B. Nelson, A. Prinz and E. Ruh, Ultra flexible SiGe/Si/Cr nanosprings, *Microelectron. J.*, 2008, **39**(3–4), 478–481.
79 J. H. Cho, T. James and D. H. Gracias, Curving Nanostructures Using Extrinsic Stress, *Adv. Mater.*, 2010, **22**(21), 2320–2324.
80 F. Liu, M. G. Lagally and J. Zang, Nanomechanical Architectures-Mechanics-Driven Fabrication Based on Crystalline Membranes, *MRS Bull.*, 2009, **34**(3), 190–195.
81 Y. F. Mei, D. J. Thurmer, C. Deneke, S. Kiravittaya, Y. F. Chen, A. Dadgar, F. Bertram, B. Bastek, A. Krost, J. Christen, T. Reindl, M. Stoffel, E. Coric and O. G. Schmidt, Fabrication, Self-Assembly, and Properties of Ultrathin AlN/GaN Porous Crystalline Nanomembranes: Tubes, Spirals, and Curved Sheets, *ACS Nano*, 2009, **3**(7), 1663–1668.
82 F. Xu, W. Lu and Y. Zhu, Controlled 3D Buckling of Silicon Nanowires for Stretchable Electronics, *ACS Nano*, 2010, **5**(1), 672–678.
83 F. Xu, W. Lu and Y. Zhu, Controlled 3D buckling of silicon nanowires for stretchable electronics, *ACS Nano*, 2011, **5**(1), 672–678.
84 Y. G. Sun, W. M. Choi, H. Q. Jiang, Y. G. Y. Huang and J. A. Rogers, Controlled buckling of semiconductor nanoribbons for stretchable electronics, *Nat. Nanotechnol.*, 2006, **1**(3), 201–207.
85 H. H. A. Ordered, Self-Organization of a Mesoscale Bristle into, *Nano Lett.*, 2006, **6**, 55.
86 J. Bico, B. Roman, L. Moulin and A. Boudaoud, Elastocapillary coalescence in wet hair, *Nature*, 2004, **432**(7018), 690.
87 B. Pokroy, S. H. Kang, L. Mahadevan and J. Aizenberg, Self-Organization of a Mesoscale Bristle into Ordered, Hierarchical Helical Assemblies, *Science*, 2009, **323**(5911), 237–240.
88 S. H. Kang, B. Pokroy, L. Mahadevan and J. Aizenberg, Control of Shape and Size of Nanopillar Assembly by Adhesion-Mediated Elastocapillary Interaction, *ACS Nano*, 2010, **4**(11), 6323–6331.
89 H. G. Duan and K. K. Berggren, Directed Self-Assembly at the 10 nm Scale by Using Capillary Force-Induced Nanocohesion, *Nano Lett.*, 2010, **10**(9), 3710–3716.
90 M. De Volder, S. H. Tawfick, S. J. Park, D. Copic, Z. Z. Zhao, W. Lu and A. J. Hart, Diverse 3D Microarchitectures Made by Capillary Forming of Carbon Nanotubes, *Adv. Mater.*, 2010, **22**(39), 4384–4389.
91 J. Yu, H. Jin, Q. Wang, X. Wei, H. Chen and Y. Wang, Coalescence of Au–Pd Nanoropes and their Application as Enhanced Electrocatalysts for the Oxygen Reduction Reaction, *Small*, 2022, **18**(44), 2203458.
92 X. Tao, H. Li, B. Yu, X. Wu, Y. Lu, Y. Wang and H. Chen, Solution synthesis of helical gold nanowire bundles, *Nanoscale*, 2019, **11**(42), 19729–19735.
93 Y. Lu, X. Cheng, H. Li, J. Zhao, W. Wang, Y. Wang and H. Chen, Braiding ultrathin Au nanowires into ropes, *J. Am. Chem. Soc.*, 2020, **142**(24), 10629–10633.
94 Y. Wang, J. He, X. Mu, D. Wang, B. Zhang, Y. Shen, M. Lin, C. Kübel, Y. Huang and H. Chen, Solution growth of ultralong gold nanohelices, *ACS Nano*, 2017, **11**(6), 5538–5546.
95 B. Yu, Q. Yang, H. Li, Z. Liu, X. Huang, Y. Wang and H. Chen, Gold nanospirals on colloidal gold nanoparticles, *J. Colloid Interface Sci.*, 2019, **533**, 304–310.
96 X. Wang, M. G. Moula, G. He, H. Jin, D. Su, J. Zong, Y. Zhang, H. Chen and Y. Wang, Alkynyl ligands-induced growth of ultrathin nanowires arrays, *J. Colloid Interface Sci.*, 2022, **627**, 640–649.
97 S. Yang, H. Li, R. Liu, C. Wang, J. Yu, S. Li, Y. Wang and H. Chen, Understanding the evolution of tunable spiral threads in homochiral Au nano-screws, *Inorg. Chem. Front.*, 2022, **9**(16), 4136–4141.
98 S. Chen, S. Li, Y. Wang, Q. Ren, Y. Feng and H. Chen, Continuous tuning the wetting growth of Au on Se nanoparticles, *J. Colloid Interface Sci.*, 2022, **618**, 451–461.
99 J. Yu, W. Wang, S. Li, B. Yu, H. Chen and Y. Wang, Synthesis of substrate-bound seaweed-like Au nanowires with amino silane coupling agents, *Chem. Commun.*, 2022, **58**(7), 989–992.
100 Z. Lam, C. Liu, D. Su, H. B. Tao, H.-Y. Wang, J. Chen, W. Xu, L. Zhang, Y. Zhu and L. Liu, Noble metal nanowire arrays as an ethanol oxidation electrocatalyst, *Nanoscale Adv.*, 2021, **3**(1), 177–181.
101 J. Liu, H. J. Dai, J. H. Hafner, D. T. Colbert, R. E. Smalley, S. J. Tans and C. Dekker, Fullerene 'crop circles', *Nature*, 1997, **385**(6619), 780–781.
102 M. Ahlskog, E. Seynaeve, R. J. M. Vullers, C. Van Haesendonck, A. Fonseca, K. Hernadi and J. B. Nagy, Ring

formations from catalytically synthesized carbon nanotubes, *Chem. Phys. Lett.*, 1999, **300**(1–2), 202–206.
103 J. F. Colomer, L. Henrard, E. Flahaut, G. Van Tendeloo, A. A. Lucas and P. Lambin, Rings of double-walled carbon nanotube bundles, *Nano Lett.*, 2003, **3**(5), 685–689.
104 L. Song, L. J. Ci, L. F. Sun, C. H. Jin, L. F. Liu, W. J. Ma, D. F. Liu, X. W. Zhao, S. D. Luo, Z. X. Zhang, Y. J. Xiang, J. J. Zhou, W. Y. Zhou, Y. Ding, Z. L. Wang and S. S. Xie, Large-scale synthesis of rings of bundled single-walled carbon nanotubes by floating chemical vapor deposition, *Adv. Mater.*, 2006, **18**(14), 1817–1821.
105 Z. P. Zhou, D. Y. Wan, Y. Bai, X. Y. Dou, L. Song, W. Y. Zhou, Y. J. Mo and S. S. Xie, Ring formation from the direct floating catalytic chemical vapor deposition, *Physica E*, 2006, **33**(1), 24–27.
106 A. Szabo, A. Fonseca, J. B. Nagy, P. Lambin and L. P. Biro, Structural origin of coiling in coiled carbon nanotubes, *Carbon*, 2005, **43**(8), 1628–1633.
107 S. L. Zhang, Optimal configurations of multiwalled carbon nanotubes, *Phys. Rev. B: Condens. Matter Mater. Phys.*, 2002, **65**(23), 235411.
108 O. Y. ZhongCan, Z. B. Su and C. L. Wang, Coil formation in multishell carbon nanotubes: Competition between curvature elasticity and interlayer adhesion, *Phys. Rev. Lett.*, 1997, **78**(21), 4055–4058.
109 L. Song, L. Ci, L. Sun, C. Jin, L. Liu, W. Ma, D. Liu, X. Zhao, S. Luo and Z. Zhang, Large-scale synthesis of rings of bundled single-walled carbon nanotubes by floating chemical vapor deposition, *Adv. Mater.*, 2006, **18**(14), 1817–1821.
110 S. L. Zhang, S. M. Zhao, M. G. Xia, E. H. Zhang and T. Xu, Ring formation of single-walled carbon nanotubes: Competition between conformation energy and entropy, *Phys. Rev. B: Condens. Matter Mater. Phys.*, 2003, **68**(24), 245419.
111 R. Martel, H. R. Shea and P. Avouris, Ring formation in single-wall carbon nanotubes, *J. Phys. Chem. B*, 1999, **103**(36), 7551–7556.
112 R. Martel, H. R. Shea and P. Avouris, Rings of single-walled carbon nanotubes, *Nature*, 1999, **398**(6725), 299.
113 B. I. Yakobson, C. J. Brabec and J. Bernholc, Nanomechanics of carbon tubes: Instabilities beyond linear response, *Phys. Rev. Lett.*, 1996, **76**(14), 2511–2514.
114 Z. J. Li, X. L. Chen, H. J. Li, Q. Y. Tu, Z. Yang, Y. P. Xu and B. Q. Hu, Synthesis and Raman scattering of GaN nanorings, nanoribbons and nanowires, *Appl. Phys. A: Mater. Sci. Process.*, 2001, **72**(5), 629–632.
115 J. K. Jian, Z. H. Zhang, Y. P. Sun, M. Lei, X. L. Chen, T. M. Wang and C. Wang, GaN nanorings: Another example of spontaneous polarization-induced nanostructure, *J. Cryst. Growth*, 2007, **303**(2), 427–432.
116 J. H. Duan, S. G. Yang, H. W. Liu, J. F. Gong, H. B. Huang, X. N. Zhao, J. L. Tang, R. Zhang and Y. W. Du, AlN nanorings, *J. Cryst. Grow.*, 2005, **283**(3–4), 291–296.
117 Y. P. Leung, W. C. H. Choy, I. Markov, G. K. H. Pang, H. C. Ong and T. I. Yuk, Synthesis of wurtzite ZnSe nanorings by thermal evaporation, *Appl. Phys. Lett.*, 2006, **88**(18), 183110.
118 C. Y. Xu, Y. Z. Liu, L. Zhen and Z. L. Wang, Disket-nanorings of $K_2Ti_6O_{13}$ formed by self-spiraling of a nanobelt, *J. Phys. Chem. C*, 2008, **112**(20), 7547–7551.
119 C. Y. Xu, J. Wu, L. X. Lv, J. X. Cui, Z. Q. Wang, Y. D. Huang and L. A. Zhen, Single-crystal $Na_2Ti_6O_{13}$ nanorings formed by self-coiling of a nanobelt, *CrystEngComm*, 2011, **13**(7), 2674–2677.
120 G. Z. Shen and D. Chen, Self-coiling of $Ag_2V_4O_{11}$ nanobelts into perfect nanorings and microloops, *J. Am. Chem. Soc.*, 2006, **128**(36), 11762–11763.
121 C. Z. Wu, H. O. Zhu, J. Dai, W. S. Yan, J. L. Yang, Y. C. Tian, S. Q. Wei and Y. Xie, Room-Temperature Ferromagnetic Silver Vanadium Oxide ($Ag_{1.2}V_3O_8$): A Magnetic Semiconductor Nanoring Structure, *Adv. Funct. Mater.*, 2010, **20**(21), 3666–3672.
122 X. Q. Wang, G. C. Xi, S. L. Xiong, Y. K. Liu, B. J. Xi, W. Yu and Y. Qian, Solution-phase synthesis of single-crystal CuO nanoribbons and nanorings, *Cryst. Growth Des.*, 2007, **7**(5), 930–934.
123 W. Y. Yang, X. M. Cheng, H. T. Wang, Z. P. Xie, F. Xing and L. N. An, Bundled Silicon Nitride Nanorings, *Cryst. Growth Des.*, 2008, **8**(11), 3921–3923.
124 N. Komatsu, T. Shimawaki, S. Aonuma and T. Kimura, Ultrasonic isolation of toroidal aggregates of single-walled carbon nanotubes, *Carbon*, 2006, **44**(10), 2091–2093.
125 Y. Wang, D. Maspoch, S. Zou, G. C. Schatz, R. E. Smalley and C. A. Mirkin, Controlling the shape, orientation, and linkage of carbon nanotube features with nano affinity templates, *Proc. Natl. Acad. Sci. U. S. A.*, 2006, **103**(7), 2026–2031.
126 A. Guo, Y. Y. Fu, L. H. Guan, Z. Zhang, W. Wu, J. Chen, Z. J. Shi, Z. N. Gu, R. Huang and X. Zhang, Spontaneously formed closed rings of single-wall carbon nanotube bundles and their physical mechanism, *J. Phys. Chem. C*, 2007, **111**(9), 3555–3559.
127 M. Sano, A. Kamino, J. Okamura and S. Shinkai, Ring closure of carbon nanotubes, *Science*, 2001, **293**(5533), 1299–1301.
128 Y. H. Wang, D. Maspoch, S. L. Zou, G. C. Schatz, R. E. Smalley and C. A. Mirkin, Controlling the shape, orientation, and linkage of carbon nanotube features with nano affinity templates, *Proc. Natl. Acad. Sci. U. S. A.*, 2006, **103**(7), 2026–2031.
129 J. Xu, H. Wang, C. C. Liu, Y. M. Yang, T. Chen, Y. W. Wang, F. Wang, X. G. Liu, B. G. Xing and H. Y. Chen, Mechanical Nanosprings: Induced Coiling and Uncoiling of Ultrathin Au Nanowires, *J. Am. Chem. Soc.*, 2010, **132**(34), 11920–11922.
130 J. Xu, H. Wang, C. Liu, Y. Yang, T. Chen, Y. Wang, F. Wang, X. Liu, B. Xing and H. Chen, Mechanical nanosprings: Induced coiling and uncoiling of ultrathin Au nanowires, *J. Am. Chem. Soc.*, 2010, **132**(34), 11920–11922.
131 L. Chen, H. Wang, J. Xu, X. Shen, L. Yao, L. Zhu, Z. Zeng, H. Zhang and H. Chen, Controlling reversible elastic deformation of carbon nanotube rings, *J. Am. Chem. Soc.*, 2011, **133**(25), 9654–9657.

132 Y. He, Y. Chen, Q. Xu, J. Xu and J. Weng, Assembly of ultrathin gold nanowires into honeycomb macroporous pattern films with high transparency and conductivity, *ACS Appl. Mater. Interfaces*, 2017, **9**(8), 7826–7833.
133 Y. Chen, Y. Wang, J. Peng, Q. Xu, J. Weng and J. Xu, Assembly of ultrathin gold nanowires: from polymer analogue to colloidal block, *ACS Nano*, 2017, **11**(3), 2756–2763.
134 X. Li, H. Wang, Q. Xu, S. Guo, J. Du, X. Liu, J. Weng and J. Xu, Ultrathin AuAg Nanofilms from Ice-Templated Assembly of AuAg Nanowires, *Adv. Mater. Interfaces*, 2018, **5**(13), 1800256.
135 A. Volodin, M. Ahlskog, E. Seynaeve, C. Van Haesendonck, A. Fonseca and J. B. Nagy, Imaging the elastic properties of coiled carbon nanotubes with atomic force microscopy, *Phys. Rev. Lett.*, 2000, **84**(15), 3342–3345.
136 A. Volodin, D. Buntinx, M. Ahlskog, A. Fonseca, J. B. Nagy and C. Van Haesendonck, Coiled carbon nanotubes as self-sensing mechanical resonators, *Nano Lett.*, 2004, **4**(9), 1775–1779.
137 X. Q. Chen, S. L. Zhang, D. A. Dikin, W. Q. Ding, R. S. Ruoff, L. J. Pan and Y. Nakayama, Mechanics of a carbon nanocoil, *Nano Lett.*, 2003, **3**(9), 1299–1304.
138 M. A. Poggi, J. S. Boyles and L. A. Bottomley, Measuring the compression of a carbon nanospring, *Nano Lett.*, 2004, **4**(6), 1009–1016.
139 P. X. Gao, W. J. Mai and Z. L. Wang, Superelasticity and nanofracture mechanics of ZnO nanohelices, *Nano Lett.*, 2006, **6**(11), 2536–2543.
140 D. Grützmacher, L. Zhang, L. Dong, D. Bell, B. Nelson, A. Prinz and E. Ruh, Ultra flexible SiGe/Si/Cr nanosprings, *Microelectron. J.*, 2008, **39**(3–4), 478–481.
141 M. Zheng and C. H. Ke, Elastic Deformation of Carbon-Nanotube Nanorings, *Small*, 2010, **6**(15), 1647–1655.
142 P. X. Gao, W. Mai and Z. L. Wang, Superelasticity and nanofracture mechanics of ZnO nanohelices, *Nano Lett.*, 2006, **6**(11), 2536–2543.
143 D. Su, Z. Lam, Y. Zheng, Y. Wang, B. Liu and H. Chen, Enhancing the Mechanical Robustness of Gold Nanowire Array *via* Sulfide-Mediated Growth, *Small Struct.*, 2022, **3**(7), 2200014.
144 S. Lu, B. Montz, T. Emrick and A. Jayaraman, Semi-supervised machine learning workflow for analysis of nanowire morphologies from transmission electron microscopy images, *Digital Discovery*, 2022, **1**(6), 816–833.
145 B. Lin, N. Emami, D. A. Santos, Y. Luo, S. Banerjee and B.-X. Xu, A deep learned nanowire segmentation model using synthetic data augmentation, *npj Comput. Mater.*, 2022, **8**(1), 88.
146 F. Mekki-Berrada, Z. Ren, T. Huang, W. K. Wong, F. Zheng, J. Xie, I. P. S. Tian, S. Jayavelu, Z. Mahfoud and D. Bash, Two-step machine learning enables optimized nanoparticle synthesis, *npj Comput. Mater.*, 2021, **7**(1), 55.
147 D. F. Williams, N. Rahimi, J. E. Smay and S. Hemmati, Optimizing silver nanowire synthesis: machine learning improves and predicts yield for a polyol, millifluidic flow reactor, *Appl. Nanosci.*, 2023, **13**(9), 6539–6552.
148 B. Mortazavi, M. Silani, E. V. Podryabinkin, T. Rabczuk, X. Zhuang and A. V. Shapeev, First-principles multiscale modeling of mechanical properties in graphene/borophene heterostructures empowered by machine-learning interatomic potentials, *Adv. Mater.*, 2021, **33**(35), 2102807.
149 A. A. Kistanov, V. R. Nikitenko and O. V. Prezhdo, Point defects in two-dimensional γ-phosphorus carbide, *J. Phys. Chem. Lett.*, 2020, **12**(1), 620–626.
150 A. R. Oganov, C. J. Pickard, Q. Zhu and R. J. Needs, Structure prediction drives materials discovery, *Nat. Rev. Mater.*, 2019, **4**(5), 331–348.
151 A. Kochaev, K. Katin, M. Maslov and R. Meftakhutdinov, AA-stacked borophene-graphene bilayer with covalent bonding: Ab initio investigation of structural, electronic and elastic properties, *J. Phys. Chem. Lett.*, 2020, **11**(14), 5668–5673.
152 E. Alibagheri, B. Mortazavi and T. Rabczuk, Predicting the electronic and structural properties of two-dimensional materials using machine learning, *Comput. Mater. Contin.*, 2021, 67.
153 O. V. Prezhdo, *Advancing physical chemistry with machine learning*, ACS Publications, 2020, vol. 11, pp.9656–9658.
154 Y.-L. Hong, Z. Liu, L. Wang, T. Zhou, W. Ma, C. Xu, S. Feng, L. Chen, M.-L. Chen and D.-M. Sun, Chemical vapor deposition of layered two-dimensional $MoSi_2N_4$, *Mater. Sci.*, 2020, **369**(6504), 670–674.
155 B. Mortazavi, B. Javvaji, F. Shojaei, T. Rabczuk, A. V. Shapeev and X. Zhuang, Exceptional piezoelectricity, high thermal conductivity and stiffness and promising photocatalysis in two-dimensional $MoSi_2N_4$ family confirmed by first-principles, *Nano Energy*, 2021, **82**, 105716.
156 Y.-H. Chang, J.-W. Jang, Y.-C. Chang, S.-H. Lee and T.-F. Siao, Gold nanohelices: a new synthesis route, characterization, and plasmonic E-field enhancement, *ACS Omega*, 2020, **5**(25), 14860–14867.
157 Z. L. Wang, Towards self-powered nanosystems: from nanogenerators to nanopiezotronics, *Adv. Funct. Mater.*, 2008, **18**(22), 3553–3567.
158 J. K. Gansel, M. Thiel, M. S. Rill, M. Decker, K. Bade, V. Saile, G. von Freymann, S. Linden and M. Wegener, Gold helix photonic metamaterial as broadband circular polarizer, *Science*, 2009, **325**(5947), 1513–1515.
159 M. Zhao, J. Niu, C. Lu, B. Wang and C. Fan, Effects of flexoelectricity and strain gradient on bending vibration characteristics of piezoelectric semiconductor nanowires, *J. Appl. Phys.*, 2021, **129**(16), 164301.
160 J. Villafuerte, X. Zhang, E. Sarigiannidou, F. Donatini, O. Chaix-Pluchery, L. Rapenne, M.-Q. Le, L. Petit, J. Pernot and V. Consonni, Boosting the piezoelectric coefficients of flexible dynamic strain sensors made of chemically-deposited ZnO nanowires using compensatory Sb doping, *Nano Energy*, 2023, **114**, 108599.
161 R. Ning, Y. Zeng, V. Rapp, B. Zhang, L. Yang, R. Prasher and X. Zheng, Thermoelectric performance of high aspect ratio double-sided silicon nanowire arrays, *J. Appl. Phys.*, 2024, **135**(9), 095001.

162 X. Zhang, J. Deng and G. Li, Twist-Angle-Controlled Nonlinear Circular Dichroism on Gold–Crystal Hybrid Metasurfaces, *Nano Lett.*, 2024, **24**(21), 6369–6375.
163 S. Pandey, K. Samanta, J. Ahuja, S. Joseph and J. Joseph, Designing a square periodic racemic helix photonic metamaterial using phase-controlled interference lithography for tailored chiral response, *Opt. Laser Technol.*, 2024, **172**, 110489.
164 Z. Lin, C. Mikhael, C. Dai and J. H. Cho, Self-Assembly for Creating Vertically-Aligned Graphene Micro Helices with Monolayer Graphene as Chiral Metamaterials, *Adv. Mater.*, 2024, 2401451.
165 F. Gao, Y. Zhang, H. You, Z. Li, B. Zou and Y. Du, Solvent-Mediated Shell Dimension Reconstruction of Core@ Shell PdAu@ Pd Nanocrystals for Robust C1 and C2 Alcohol Electrocatalysis, *Small*, 2021, **17**(32), 2101428.
166 Y. Zhang, F. Gao, H. You, Z. Li, B. Zou and Y. Du, Recent advances in one-dimensional noble-metal-based catalysts with multiple structures for efficient fuel-cell electrocatalysis, *Coord. Chem. Rev.*, 2022, **450**, 214244.
167 Y. Wang, Y. Yuan and H. Huang, Recent advances in pt-based ultrathin nanowires: synthesis and electrocatalytic applications, *Chin. J. Chem.*, 2021, **39**(5), 1389–1396.
168 F. Gao, Y. Zhang, Z. Wu, H. You and Y. Du, Universal strategies to multi-dimensional noble-metal-based catalysts for electrocatalysis, *Coord. Chem. Rev.*, 2021, **436**, 213825.
169 J. Xu, B. Hong, X. Peng, X. Wang, H. Ge and J. Hu, Preparation and magnetic properties of gradient diameter FeCoNi alloys nanowires arrays, *Chem. Phys. Lett.*, 2021, **767**, 138368.
170 X. Chen, W. Wang, X. Chen, X. Liao, Z. Lyu, K. Liu and S. Xie, Structure-intensified PtCoRh spiral nanowires as highly active and durable electrocatalysts for methanol oxidation, *Nanoscale*, 2021, **13**(4), 2632–2638.
171 Y. Mo, S. Feng, T. Yu, J. Chen, G. Qian, L. Luo and S. Yin, Surface unsaturated WOx activating PtNi alloy nanowires for oxygen reduction reaction, *J. Colloid Interface Sci.*, 2022, **607**, 1928–1935.
172 Q. Chang, D. Yang, X. Zhang, Z. Ou, J. Kim, T. Liang, J. Chen, S. Cheng, L. Cheng and B. Ge, Understanding ZIF particle chemical etching dynamics and morphology manipulation: *in situ* liquid phase electron microscopy and 3D electron tomography application, *Nanoscale*, 2023, **15**(33), 13718–13727.
173 X. Song, X. Zhang, Q. Chang, X. Yao, M. Li, R. Zhang, X. Liu, C. Song, Y. X. A. Ng and E. H. Ang, High-Resolution Electron Tomography of Ultrathin Boerdijk–Coxeter–Bernal Nanowire Enabled by Superthin Metal Surface Coating, *Small*, 2022, **18**(41), 2203310.
174 D. Yang, Y. X. A. Ng, K. Zhang, Q. Chang, J. Chen, T. Liang, S. Cheng, Y. Sun, W. Shen and E. H. Ang, Imaging the surface/interface morphologies evolution of silicon anodes using *in situ*/operando electron microscopy, *ACS Appl. Mater. Interfaces*, 2023, **15**(17), 20583–20602.
175 Q. Chang, Y. X. Angel Ng, D. Yang, J. Chen, T. Liang, S. Chen, X. Zhang, Z. Ou, J. Kim and E. H. Ang, Quantifying the morphology evolution of lithium battery materials using operando electron microscopy, *ACS Mater. Lett.*, 2023, **5**(6), 1506–1526.
176 Y. Sun, X. Zhang, R. Huang, D. Yang, J. Kim, J. Chen, E. H. Ang, M. Li, L. Li and X. Song, Revealing microscopic dynamics: *in situ* liquid-phase TEM for live observations of soft materials and quantitative analysis *via* deep learning, *Nanoscale*, 2024, **16**(6), 2945–2954.
177 N. Han, M. Sun, Y. Zhou, J. Xu, C. Cheng, R. Zhou, L. Zhang, J. Luo, B. Huang and Y. Li, Alloyed palladium–silver nanowires enabling ultrastable carbon dioxide reduction to formate, *Adv. Mater.*, 2021, **33**(4), 2005821.
178 Y. Wang, H. Lv, L. Sun, X. Guo, D. Xu and B. Liu, Ultrathin and wavy PdB alloy nanowires with controlled surface defects for enhanced ethanol oxidation electrocatalysis, *ACS Appl. Mater. Interfaces*, 2021, **13**(15), 17599–17607.
179 H. Yu, T. Zhou, Z. Wang, Y. Xu, X. Li, L. Wang and H. Wang, Defect-rich porous palladium metallene for enhanced alkaline oxygen reduction electrocatalysis, *Angew. Chem., Int. Ed.*, 2021, **133**(21), 12134–12138.
180 J. Li, Z. Zhou, H. Xu, C. Wang, S. Hata, Z. Dai, Y. Shiraishi and Y. Du, *In situ* nanopores enrichment of Mesh-like palladium nanoplates for bifunctional fuel cell reactions: A joint etching strategy, *J. Colloid Interface Sci.*, 2022, **611**, 523–532.
181 S. Liu, H. Ren, S. Yin, H. Zhang, Z. Wang, Y. Xu, X. Li, L. Wang and H. Wang, Defect-rich ultrathin AuPd nanowires with Boerdijk–Coxeter structure for oxygen reduction electrocatalysis, *Chem. Eng. J.*, 2022, **435**, 134823.
182 S. Liu, S. Yin, Z. Wang, Y. Xu, X. Li, L. Wang and H. Wang, AuCu nanofibers for electrosynthesis of urea from carbon dioxide and nitrite, *Cell Rep. Phys. Sci.*, 2022, **3**(5), 100869.
183 H. You, F. Gao, C. Wang, J. Li, K. Zhang, Y. Zhang and Y. Du, Rich grain boundaries endow networked PdSn nanowires with superior catalytic properties for alcohol oxidation, *Nanoscale*, 2021, **13**(42), 17939–17944.
184 L. Sahoo, R. Garg, K. Kaur, C. Vinod and U. K. Gautam, Ultrathin twisty PdNi alloy nanowires as highly active ORR electrocatalysts exhibiting morphology-induced durability over 200 K cycles, *Nano Lett.*, 2022, **22**(1), 246–254.
185 Q. Xue, X.-Y. Bai, Y. Zhao, Y.-N. Li, T.-J. Wang, H.-Y. Sun, F.-M. Li, P. Chen, P. Jin and S.-B. Yin, Au core-PtAu alloy shell nanowires for formic acid electrolysis, *J. Energy Chem.*, 2022, **65**, 94–102.
186 J. Wang, X. Zhang, M. Zhang, P. Zhang, Y. Song and J. Zhang, Facile synthesis of trimetallic Au@ PdPt nanowires-networks with *in situ* Au nanowires as templets for methanol oxidation, *Mater. Lett.*, 2021, **305**, 130823.
187 J. Wong-Leung, I. Yang, Z. Li, S. K. Karuturi, L. Fu, H. H. Tan and C. Jagadish, Engineering III–V semiconductor nanowires for device applications, *Adv. Mater.*, 2020, **32**(18), 1904359.
188 C.-Y. Hsu, A. M. Rheima, Z. Sabri Abbas, M. U. Faryad, M. M. Kadhim, U. S. Altimari, A. H. Dawood, Z. T. Abed, R. S. Radhi and A. S. Jaber, Nanowires properties and applications: a review study, *S. Afr. J. Chem. Eng.*, 2023, **46**, 286–311.